KfK 4938
CNEA 17/91
Dezember 1991

Deformation and Rupture Behavior of Argentine Zircaloy-4 Cladding Tubes in the Temperature Range from 700 to 1200 °C at Different Heating Rates in Inert Atmosphere

M. E. Markiewicz, F. J. Erbacher
Institut für Angewandte Thermo- und Fluiddynamik
Institut für Materialforschung
Projekt Nukleare Sicherheitsforschung

Kernforschungszentrum Karlsruhe

KERNFORSCHUNGSZENTRUM KARLSRUHE

Institut für Angewandte Thermo- und Fluiddynamik
Institut für Materialforschung
Projekt Nukleare Sicherheitsforschung

KfK 4938
CNEA 17/91

DEFORMATION AND RUPTURE BEHAVIOR OF ARGENTINE ZIRCALOY-4 CLADDING TUBES IN THE TEMPERATURE RANGE FROM 700 TO 1200°C AT DIFFERENT HEATING RATES IN INERT ATMOSPHERE

M.E. Markiewicz*, F.J. Erbacher

* Comision Nacional de Energia Atomica, Centro Atomico Constituyentes, Buenos Aires, Argentina

Kernforschungszentrum Karlsruhe GmbH, Karlsruhe

Kernforschungszentrum Karlsruhe GmbH
Postfach 3640, 7500 Karlsruhe 1

ISSN 0303-4003

DEFORMATION AND RUPTURE BEHAVIOR OF ARGENTINE ZIRCALOY-4 CLADDING TUBES IN THE TEMPERATURE RANGE FROM 700 TO 1200°C AT DIFFERENT HEATING RATES IN INERT ATMOSPHERE

ABSTRACT

In the tube burst apparatus TUBA burst tests were performed at CNEA/CAC-Buenos Aires in short Zircaloy-4 tube specimens.

The main objective was to investigate the deformation and burst behavior of Argentine cladding tubes and to compare it with data obtained by others.

It was found that the burst data e.g. burst temperature and circumferential burst strain and the influence of different heating rates are in good agreement with those from other origin.

VERFORMUNGS- UND BERSTVERHALTEN ARGENTISCHER ZIRCALOY-4 HÜLLROHRE IM TEMPERATURBEREICH ZWISCHEN 700 UND 1200°C UNTER SCHUTZGAS BEI UNTERSCHIEDLICHEN AUFHEIZRATEN

ZUSAMMENFASSUNG

In der Rohrberstversuchsanlage TUBA (Tube Burst Apparatus) wurden bei CNEA/CAC-Buenos Aires Berstversuche an kurzen Zircaloy-4-Rohrabschnitten durchgeführt.

Die wesentliche Zielsetzung war die Untersuchung des Verformungs- und Berstverhaltens von Hüllrohren aus argentinischer Herstellung und sein Vergleich mit dem aus anderen Ländern.

Ein Vergleich der ermittelten Berstdaten wie z.B. Bersttemperatur und Berstdehnung sowie deren Beeinflussung durch unterschiedliche Aufheizraten ergab eine gute Übereinstimmung mit den Berstdaten von Zircaloy-4 Hülllrohren aus anderer Herstellung.

CONTENTS

1. INTRODUCTION

In this work the results are presented of experiments carried out under temperature transient conditions in the range of 700 to 1200°C with tubes made of Zircaloy-4. Such temperatures could be reached in the case of a loss-of-coolant accident (LOCA) occurring in a Pressurized Heavy Water Reactor (PHWR), where rapid depressurization of the cooling system is followed by increasing temperatures in the fuel claddings.

The temperature range was chosen on the assumption that at around 700°C the first fuel cladding would fail as a consequence of the internal overpressure and that 1200°C may be reached which constitutes the maximum temperature allowed by the emergency core cooling criteria.

The deformation and rupture behavior of Zircaloy-4 tubes subjected to temperature ramps were studied by simulating the thermal excursion associated with a LOCA, when the strength of the Zircaloy cladding falls rapidly below the values required to withstand the stresses resulting from the internal overpressure. The combination of low mechanical strength and high differential pressure across the cladding results in softening, plastic deformation and, finally, rupture of the cladding.

The results obtained contribute to the knowledge of the ballooning behavior in fuel claddings under specified conditions of internal pressures and heating rates. It was not attempted to simulate the real cladding loading during a LOCA.

The main objective of this work was to obtain information on the ballooning characteristics in Zircaloy-4 claddings fabricated in Argentina, so as to be able to compare the results with values obtained by others and to provide the database for incorporating the information into the fuel modeling codes.

The results obtained are presented graphically. They cover a range of temperatures which is of interest in studies of a LOCA and thus allow a comparison to be made with other experimental results.

2. MATERIAL, APPARATUS AND EXPERIMENTAL PROCEDURE

The internally pressurized Zircaloy-4 tubes were exposed to a constant heating rate in order to produce diametral strains and rupture at temperatures between 700 to 1200°C.

The tubes used in this experimental work were supplied by CONUAR S.A. according to specifications for the cladding tubes used at the PHWR Atucha I. Their nominal dimensions were: 11.9 mm outside diameter, 0.55 wall thickness.

The length of the tubes tested was 130 mm. They were closed at one end with a TIG welded plug; the opposite end was connected to the pressurization system. There was no axial restriction.

The specimens were heated by an external electrical heater in a concentric arrangement with the tube. The temperature was adjusted by a programmable electronic system controlling a power unit which was connected in series to the transformer. This regulator is controlled by two chromel-alumel thermocouples placed in the heater and in the specimen, respectively.

Figure 1 shows a diagram of the equipment used to perform the experiments; it basically consists of a vacuum and pressurization system, a temperature programmer capable of selecting the ramps, maximum temperatures and time, a video system to film the circumferential strain and record the temperature, pressure and time values, and a 30 kW power generator to feed the heater.

The specimen temperature was controlled by two chromel-alumel thermocouples placed at the same elevation and diametrically opposite in order to estimate the azimuthal temperature difference. The difference of the instantaneous values measured was less than 8 K and diminished with decreasing heating rate.

The pressure inside the tube was measured with a pressure transducer placed near the specimen. The pressure and temperature signal were simultaneously recorded and superposed to the video signal through a character generator; the timer signal was also coupled. The values were recorded on a video tape for later reproduction.

After the specimen was installed and instrumented, the heater system was surrounded by a chamber (see Fig. 1), connected to the vacuum system and evacuated down to a value of 7×10^{-5} mbar. Afterwards, the chamber was pressurized up to 500 mbar.

The specimen was pressurized and depressurized several times with argon in order to evacuate the air contained and then placed in line with the pressure reservoir loaded up to the desired value. During the experiment, the pressure was kept constant. This was possible due to the large volume of the pressure tank compared to the specimen volume.

Once the temperature had become stabilized at 300°C during 10 minutes, the specimen was pressurized, the filming equipment was started and the experiment begun at the selected heating rate, that was constant in each test till the cladding failed which could be seen at the monitor.

A video camera continuously recorded the tube deformation at its axial midplane from the start of heat-up until rupture. The tube diameter was measured on the monitor ($\times 8$) with a graduated scale.

When the experiment was finished, the video recorder reproduced every 0.02 s the image and the values of heating rate, instantaneous temperature, pressure, time, and increase in diameter obtained from the monitor. A typical plot of a transient test is shown in Fig. 2.

The experiments were carried out in the range of pressures from 3 – 130 bar and at heating rates of 1,7 and 15 K/s in argon atmosphere.

After cooling the specimen was removed from the furnace and the circumferential strain (in the rupture zone), axial strain (taking $L_0 = 50$ mm as initial length), and the maximum wall thickness in the zone of maximum circumferential strain were measured.

3. RESULTS

3.1 Circumferential Deformation

The data obtained from the experiments showed a very good reproducibility of the results in the range of pressures examined and at the different heating rates. The values are listed in Tables 1, 2, and 3.

The development of the diametrical strain with time of tubes internally pressurized and heated at a rate of 7 K/s is shown in Figs. 3, 4 and 5 for different specimens. The diametral strain rate derived from the slope of strain vs. time is also shown.

This deformation process is characterized by an initial period when the diametral strain rate is relatively low while the temperature increases. This stage lasts until the temperature level is reached which is necessary to produce approximately 5 to 10% diametral strain. Then, the strain rate from 10% deformation till rupture is high, increasing abruptly during the last second before rupture.

From the observation of the continuous record of deformation as function of temperature and time it is evident that the transition from uniform deformation to local ballooning is not an abrupt process, but rather a process developing in the last phase prior to rupture where the larger part of diametral strain occurs at the highest temperature for a given pressure. This localization in deformation occurs during the last 2 seconds, approximately, before the cladding fails.

3.2 Radial Instability

During the process of cladding deformation, which takes place at pressure and ramps of temperature, two different types of instability associated with the deformation process can be observed. The first is a longitudinal localization of circumferential deformation which gives rise to ballooning. The second type of instability is that associated with the localized strain in the wall thickness and it takes place after considerable circumferential deformation.

Referring to the criterion developed by Franklin (1) and used by Chung and Kassner in their experiments (2), it was tried to determine the moment and the circum-

ferential strain of the instability. It was not possible to obtain the following relation for the whole range of deformation:

$$\frac{d\ ln\ \varepsilon_d}{dt} > \frac{2d\ ln\ \varepsilon_d}{dt}$$

ε_d: diametral strain

In other words, it was not possible to identify a point associated with the change from uniform deformation to localized deformation.

To determine the moment at which the second type of instability is produced, it was considered that thinning of the wall thickness was uniform along the circumference of the tube (even for a high circumferential strain) till the moment at which the localization in the radial strain was produced. Once this localization is established, the circumferential stress acting in the unlocalized sector is lower than in the thinned part of the tube; therefore, no larger deformations are expected in this region until rupture occurs.

The instability of the wall thickness was determined by measuring the wall thickness. For this, metallographic cross-sections in the zone of maximum circumferential strain were used. With the maximum wall thickness value, the circumferential deformation reached for the tube before producing the localization in the wall thickness was calculated.

For this calculation the procedure detailed in the appendix was used, by which the following relations were obtained:

$$\delta_{ci} = \frac{D_i - D_o}{D_o} \cdot 100 \qquad (1)$$

$$D_i = \frac{\Delta A \cdot D_{mo} \cdot e_o + e_f^2}{e_f} \qquad (2)$$

where:

- δ_{ci}: circumferential strain at instability
- D_i: outside tube diameter at the moment of instability
- D_o: initial outside diameter
- ΔA: change in the cross-sectional area

D_{mo}: initial medium diameter
e_0: initial wall thickness
e_f: maximum wall thickness measured in the ballooning zone

To calculate the outside tube diameter at the moment of intability, the increase in the cross-sectional area as a consequence of the shortening suffered by the tube was considered. This increase in the area was calculated under the following assumptions:

1. The total shortening of the tube medium line is produced as soon as the localization of the deformation in the wall thickness begins.
2. The increase in the transversal area is homogeneously distributed along the length of ballooning.

To demonstrate the effect of the axial strain, estimations of the cross-sectional area (using the formula 6 in the appendix) show an increase in the area of up to 25% for claddings that have experienced a high axial strain. This rise results from the contribution of the material flow to the deformed region due to axial shortening.

The error made in determination of the outside diameter reached at the moment of instability, due to the suppositions 1 and 2 is negligible in the experiments where the tube has ruptured at the temperatures at which Zircaloy reaches the β phase. The reason is that the shortening suffered by the tubes in this zone was not more than 4%. This is shown in Fig. 6 for the three heating rates demonstrating that a large increase in the cross-sectional area is not expected. In no case was axial elongation observed.

This figure shows the pronounced shortening of the tube that has been ruptured in the α-phase to accommodate the large circumferential strain.

The claddings in the α-phase are strongly textured, with the basal axis orientated in the radial direction. The limited slip system that operates in the hexagonal-closely packed crystal structure (hcp) results in a pronounced mechanical anisotropy. Slip on prisms and basal planes has been reported by Tenckhoff (3) and, in either case, the Burgers vector is parallel to the basal plane. Therefore, the circumferential expansion must be accomodated to some extent by axial contraction

since the tube resists accommodation of tangential expansion solely by wall thinning.

On the other side, β-Zircaloy being essentially isotropic, accommodates the circumferential strain primarly by wall thinning.

From the 90 experiments carried out it was determined that the instability in the wall thickness occurs between 0.2 and 0.04 seconds before rupture, at a high circumferential strain and when the diametral strain rate is already high; see Figs. 3,4 and 5.

This analysis which was made to find the instability in the wall thickness, is valid for the experiments carried out without azimuthal temperature differences (A.T.D.). They produce larger differences in the wall thickness between the opposite side and the burst tip (4), resulting in a lower total circumferential strain.

3.3 Effect of the Heating Rate

The influence of different heating rates on the deformation behaviour, strength and rupture of Zircaloy claddings was analyzed at heating rates of 1, 7 and 15 K/s. Figures 7, 8 and 9 show the circumferential deformation at rupture as a function of burst temperature for the different heating rates. The limits indicating the phase changes only serve as reference because their values apply to a process carried out under equilibrium conditions.

The scatter in the experimental data is attributed mainly to azimuthal temperature differences, considering the high sensitivity in Zircaloy cladding deformation with little variations of temperature, heating rate and local imperfection in the tube wall.

It can be observed that, at the heating rates tested, the circumferential strain produces two maxima, the first at the highest temperature in the α-zone and the second when the Zircaloy is exposed to the lowest temperatures in the β-phase. The minimum of deformation is in the α + β-transition zone, whose limits are 820 and 980 °C at approximate in equilibrium conditions.

These values shift to higher temperatures when the heating rate increases. D. Hardy (5) found that, with a heating rate of 25 K/s, the $\alpha \rightarrow \alpha + \beta$ is shifted to 840 °C and. at 100 K/s to 854 °C.

The relative amount of α and β in the two-phase regions changes with the temperature. Thus, during the temperature transient in this region a continuous phase transformation is produced by which the α-phase fraction existing in the $\alpha/\alpha + \beta$ equilibrium line increases with increasing heating rates. Therefore, the anisotropic behaviour is more pronounced for the specimens heated at the higher heating rates.

The results show that the rupture strains are dependent on the heating rate in a large range of temperatures, with changes in the temperatures at the maximum and minimum deformation values (figure 10). The change in the burst temperature is much higher in the single-phase zone than in the transition zone. This could be a consequence of the $\alpha \rightarrow \beta$ transformation which is endothermic and could result in reducing or equilizing the heating rate effect when the material passes through this zone (6).

The first maximum deformation decreases and shifts to higher temperatures when the heating rate increases at the heating rates tested. The variation of the strain peak height with the heating rate is thought to be primarily due to the strain rate.

At high heating rates the deformation could be considered only on the basis of short-term mechanical properties, while at low heating rates, the contribution by creep becomes important. It allows the tube to reach a given strain at relatively lower temperatures.

The dependence of the maximum deformation on the temperature and the height of the strain peak on the heating rate can be explained on the basis of strain rate and microstructure considerations.

The strain rate hardening of the material increases as the heating rate increases. This means that less time is available for annealing and relaxation of the cladding. Therefore, a higher temperature is required to achieve the same amount of deformation before failure is produced. As a result at higher heating rates large deformations will occur at higher temperatures.

In the three heating rates investigated, the temperature at which the first maximum strain is produced coincides with the temperature of the maximum axial strain. This shortening, in the α-phase, follows the circumferential deformation, and its maximum value decreases with increasing heating rate.

As for the ductility minimum, it was observed that the α to β-phase transformation has a great influence on the deformation of Zircaloy. However the effect of such transformation on deformation has not yet been clarified.

Hobson et al. (7) found that the α+ β transformation is a diffusionless shear process, providing a free deformation mechanism directed by the stresses applied. Thus, work hardening would be a minimum in this two-phase region promoting an early rupture with low uniform deformation.

In the present experiments the estimations of the uniform deformation in the wall thickness show a considerable reduction in the values; this is even more pronounced in the experiments performed at the higher heating rates. The uniform radial deformation (wall thickness) was calculated by measuring the initial wall thickness and maximum wall thickness in the tube cross-section after the rupture.

These results confirm that the large reduction in the circumferential strain in the two-phase region is a premature localization of circumferential strain rather than a reduction of the localized strain required for rupture.

The second peak of maximum deformation occurs when the tube is loaded at low pressure, allowing the Zircaloy to reach the β-phase. Figure 10 shows that at the tested heating rates there was no influence on the maximum deformation values, but as in the case of the specimens bursting in the α-phase, the maximum strain shifts to higher temperatures with increasing heating rate.

In Fig. 10 the line of maximum circumferential strain at the moment of wall thickness instability is shown together with the maximum circumferential rupture strain curves. The values were estimated using Eq. 1.

This figure enables to establish the percentage of the circumferential rupture strain at which the radial instability occurs as well as the ratio of the localized radial strain to the total circumferential strain in the whole range of temperatures.

The differences between both deformations, (rupture and instability), are similar in the α and β-zones for the three heating rates.

For the tubes failed in the α-phase region, or at the low temperatures in the α → β-transition zone, the localized thinning of the wall thickness provides a low percentage of the total strain; it is estimated at approximately 12 %. This low value is a consequence of the high uniform strain acting on the wall thickness and the high axial shortening in this zone. Metallographic examinations show also that the difference in the wall thickness between the fracture adjacent zone and the opposite rupture side is not big, which leads to the conclusion that the contribution of the local radial deformation to the total strain is little.

On the other side, in the claddings which reached burst temperatures in the β-phase or preponderantly β-phase in the transition zone, the ratio of the localized radial strain to the total strain is higher than that for the specimens burst in the α-zone, producing the radial instability at a circumferential burst strain of approx. 70 %.

This high contribution is a consequence of localized radial deformations developing along the cladding circumference. Figure 11 is a comparison between two tubes which suffered similar rupture strain, but failure of one of them occurred in the α-phase (A), while the other failed in the β-phase (B). The cross-section in the rupture zone and a magnification of the side opposite to burst show the localized deformation produced in the tube that reached the higher rupture temperature, whereas wall thinning progresses towards the rupture end in the tube burst in the α-phase.

These localized radial deformations increase with the circumferential strain producing, in some cases, a failure with more than one burst opening around the circumference; see photographs in Fig. 12.

In Fig. 13 A, which gives the maximum wall thickness distribution in the rupture zone as a function of burst temperature, and in Fig. 13B that compares axial shortenings of the tubes at different heating rates, three zones can be observed in the plot of circumferential deformation vs. burst temperature; (see Fig. 10). These zones are differentiated by the contribution of the circumferential and axial deformation components to the total circumferential strain, and their limits are dependent on the heating rate.

For temperature lower than approx. 880 °C the change in the maximum wall thickness as a function of the burst temperature does not exhibit a large difference at the three heating rates, but a big difference in axial shortening becomes apparent.

A large reduction in the radial deformation gets manifest in the range of temperatures from 880 to 1000 °C. This inability to deform radially increases with increasing heating rate; the same occurs with the axial strain, which is considerably reduced at the three heating rates.

From approximately 1000 °C on, the axial strain is still low, but the radial strain increases again, and is larger with the heating rate increasing and reaches values of radial deformation higher than those obtained in the α-zone.

Analyzing the deformation behaviour in these three zones, one can state that for the first zone ($T < 880$ °C) the high total strain is a consequence of the contribution by both deformations, axial and radial, while for the specimen burst in the high temperature region ($T > 1000$ °C) the total circumferential strain is determined by the contribution of the radial deformation.

The reduction in both types of deformation prevents higher rupture strains from occuring at the temperatures in the medium zone.

The dependence of the burst pressure from burst temperature at the various heating rates has been plotted in Fig. 14. The heating rate shows its effect in the whole range of pressures, suggesting that the highest strain rate, associated with the highest heating rate, results in higher burst temperatures.

The curves show the change in the slope near the transition zone $(\alpha + \beta) \rightarrow \beta$. At temperatures higher than that in this interphase, small variations in the internal pressure cause large changes in the temperature at rupture. At temperatures lower than that in the transition zone $\alpha \rightarrow (\alpha + \beta)$, the curves show a small shift in the temperature at which rupture occurs, provided that the pressure is varied. This is the range of temperatures where the Zircaloy greatly decreases in strength when the temperature is increased.

With the rupture pressure values and using the following expression, the circumferential stress at the moment of instability in the wall thickness was determined:

$$\sigma_{0i} = P\left(\frac{1}{20} + \frac{\Delta A \cdot K}{e_i^2}\right) \qquad \textit{(see appendix)}$$

σ_{0i}	=	circumferential stress at radial instability, MPa
P	=	pressure, bar
ΔA	=	increase in the cross-sectional area
K	=	constant, dependent on tube dimension
e_i	=	maximum wall thickness in the rupture zone

These values of Tables 1, 2 and 3 are shown in Figs. 15, 16 and 17. Figure 18 shows the medium line of each curve for intercomparison of the different heating rates.

The experiments carried out at higher heating rates resulted in a higher stress at instability in a large range of temperatures. These results confirm the data of Fig. 14 that indicate the increase in the burst strength with the higher heating rate.

The increase in instability stress with the heating rate shows a zone where the differences disappear. This occurs in the range of temperatures from 880 to approx. 1040 °C. There is also a large decrease in the uniform radial strain (Fig. 13 A) with the resulting reduction in the stresses at the moment of instability.

Figure 19 shows that the type of fracture changes with the increase in the burst temperature. The area of burst opening was large at the lower temperatures, while in those bursting at higher temperatures the tubes were only partly opened. The difference is due to the greater quantity of energy stored in the specimens failing at low temperatures. The tubes burst in the β-phase had an orange peel appearance as a consequence of the combination of deformation and fast grain growth in the β-phase.

The axial distribution of the circumferential strain was reproducible in all experiments. The tubes develop a conical shape at both sides of ballooning, with small circumferential deformations, limiting ballooning to a short axial length. This is because, by external heating, the cladding temperature in the ballooning zone increases as deformation increases. This implies that the regions neighbouring bal-

looning reach lower temperatures, with the consequential destabilizing effect in the deformation process, thus avoiding the propagation of circumferential strains in the axial direction.

The dependence of burst temperature on the heating rate is again demonstrated in Fig. 20 for internal pressures between 6 and 100 bar. The curves indicate that the effect of the heating rate is not modified in the range of pressures and temperatures examined.

4. Comparison with other Results

One of the objectives of this work was to compare the behaviour of Argentine claddings with the results obtained in previous works performed at various laboratories under similar test conditions. The small variations observed can be attributed to experimental and material differences such as the heating rate, atmosphere (vacuum or argon), temperature measurement, heating method, azimuthal temperature difference, differences in thermal and mechanical treatments, etc.

Figures 21, 22 and 23 show by way of comparison the burst circumferential strains as a function of the burst temperature for different heating rates.

In Figs. 24, 25 and 26 the initial circumferential stresses are presented as a function of burst temperatures. This presentation is more meaningful because it allows to eliminate the dimensional effect in the design specifications which is not possible when the burst pressure is compared with the burst temperature. These figures show the tendency of the burst temperature to increase with increasing heating rates when the tubes are exposed to the same initial circumferential stress.

The comparison demonstrates that the results obtained with the Argentine claddings are in reasonable agreement with the results of other experimental work carried out under similar conditions.

5. Conclusions

The deformation and rupture behaviour of Zircaloy-4 claddings made in Argentina were studied in argon atmosphere and exposed to various heating rates which are of interest in a design basis LOCA in a PHWR. The effect of internal pressure and heating rate on the circumferential deformation was determined in the range of temperatures from 700 to 1200 °C.

The following conclusions can be drawn from results of this work:

- The almost total circumferential strain develops during the last two seconds before the rupture, with a fast increase in the diametral strain rate between 0.4 and 0.15 s before the tube fails.

- The criterion developed to determine the radial instability shows that the localization of the wall thickness deformation occur between 0.2 and 0.04 s before the burst.

- The contributions of radial and axial deformations to the total deformation differ depending on whether rupture occurs in the α- or β-zone. In the α-zone, the axial shortening increases with the increase in the circumferential strain.

- With increasing heating rates the temperature required to produce a given deformation is shifted towards higher values. The largest effect occur in the single phase regions. The height of the circumferential burst strain peak decreases in the α-phase with an increasing heating rate.

- A minimum of the circumferential strain was found in the α + β-zone for all the heating rates.

- For a given internal pressure, the increase in the heating rate produces a rise in the burst temperature.

- The analysis of the results shows that the transient deformation behaviour of the Argentine claddings is comparable to those of previous works.

References

/1/ D. Franklin, Acta metallurgica, Vol. 20, June 1972

/2/ H.M. Chung, T.F. Kassner, "Deformation Characteristics of Zircaloy Cladding in Vacuum and Steam Under Transient Heating Conditions", NUREG/CR - 0347, ANL-77-31

/3/ E. Tenckhoff, "Operable Deformation System and Mechanical Behaviour of Textured Zircaloy Tubing". ASTM STP 551, pp. 179-200, (1974)

/4/ M.E. Markiewicz, F.J. Erbacher, "Experiments on Ballooning in Pressurized and Transiently Heated Zircaloy-4 Tubes". KfK 4343, February 1988

/5/ D. Hardy, "High Temperature and Rupture Behaviour of Zircaloy Tubing", ANS Topical Meeting on Water Reactor Safety, Salt Lake City, Utah, 1973, 254-272.

/6/ D.O. Hobson, "Comparison of Rupture Data From Irradiated Fuels Rods and Unirradiated Cladding". Nuclear Technology, Vol. II, p. 479, May 1971.

/7/ K.M. Emmerich, "Failure of Pressurized Zircaloy Tubes During Thermal Excursion in Steam and in Inert Atmospheres", ASTM STP 458, pp. 252-268, 1969

/8/ D.B. Clay, T. Healey, "Deformation and Rupture of Zircaloy Tubes During Transient Heating". Meeting on the Behaviour of Water Reactor Fuel Elements under Accident Conditions, Spatind, Norway, 12th-16th September, 1976.

/9/ A.A. Bauer, "Evaluating Strength and Ductility of Irradiated Zircaloy", BMI-NUREG 1985, NRC-3, October 1977

Appendix

During the process of deformation of pressurized tubes exposed to ramps of temperature an abrupt change was observed in the diametral strain rate immediately before the rupture. This increase in the strain rate is produced when the circumferential deformation has already reached a high value so that the strain rate associated with the first type of instability does not occur.

To determine the moment at which the second type of instability is produced (localization of wall thickness deformation) and the circumferential strain reached at that instant, the following procedure was developed:

initial cross-sectional area:

$$A_o = \pi \cdot D_{m.o} \cdot e_o \tag{1}$$

cross-sectional area at the moment of instability:

$$A_i = \pi \cdot D_{m.i.} \cdot e_i \tag{2}$$

$D_{m.o.}$: initial medium diameter
$D_{m.i.}$: medium diameter at instability
e_o : initial wall thickness
e_i : wall thickness at instability

Due to the shortening suffered by the tubes, the area A_i should increase

$$A_i > A_o \tag{3}$$

By volume conservation

$$V_o = V_i = A_o \cdot L_o = A_i \cdot L_f \tag{4}$$

V_o : initial volume
V_i : volume at instability
L_o : initial length, 50 mm
L_f : final length, measured after burst

In (4), two assumptions were made:

a - The total shortening of the tube medium line is produced at the moment when the localization of the deformation in the wall thickness begins.

b - The increase in the cross-sectional area is homogeneously distributed along the length of ballooning.

Then

$$A_i = \frac{A_o \cdot L_o}{L_f} \tag{5}$$

The cross-sectional area increases as follows:

$$\Delta A = \frac{A_i}{A_o} \tag{6}$$

$$\Delta A(\%) = \frac{A_i - A_o}{A_o} \cdot 100$$

Replacing 1 and 2 in 6 one obtains:

$$D_{m.i.} = \frac{\Delta A \cdot D_{m.o.} \cdot e_o}{e_i} \tag{7}$$

The external diameter at the moment of instability is:

$$D_i = D_{m.i.} + e_i = \frac{\Delta A \cdot D_{m.o.} \cdot e_o + e_i^2}{e_i} \tag{8}$$

The e_i-value is obtained by measurement of the maximum wall thickness in the zone of maximum circumferential deformation after rupture assuming that no larger radial deformations are expected in the unlocalized region (normally opposite the burst region) between the instability and the moment of rupture.

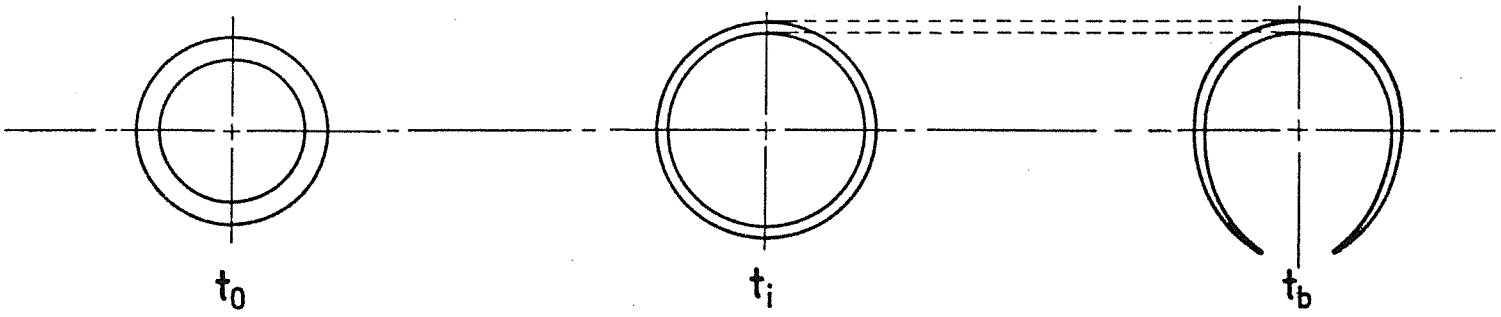

With the value of the diameter obtained in (8), the circumferential deformation reached at the moment of radial instability is calculated:

$$\delta_i = \frac{D_i - D_o}{D_o} \tag{9}$$

To determine the circumferential stress at instability. the following expression was used:

$$\sigma_{\theta i} = \frac{P \cdot D_i}{20 \cdot e_i} \tag{10}$$

Replacing 8 in 10 one obtains:

$$\sigma_{\theta i} = P\left(\frac{1}{20} + \frac{\Delta A \cdot K}{e_i^2}\right) \tag{11}$$

σ_{0i} (MPa): circumferential stress at radial instability

P (Bar): burst pressure

K: constant dependent on tube dimension

Specimen N°	Burst Pressure (Bar)	Burst Temp. (°C)	Burst Strain (%)	Axial Strain (%)	Initial Stress (MPa)	Maximum Wall Thickness (mm)	Stress at Instability (MPa)
109	3	1158	72	-1,4	3,42	0,40	6
108	4	1135	78	- 2	4,56	0,37	10
111	4	1090	56	-0,8	4,56	0,45	6,5
112	4	1158	77	-6,3	4,56		
110	5	1050	96	-3,2	5,7	0,36	13
107	7	1030	103	-3,1	7,98		
106	8	1010	83	-1,1	9,12		
105	10	1007	71	-3,9	11,4	0,41	20
104	10	1000	95	-2,8	11,4		
103	12	980	75	-1,9	13,68		
102	12	975	25	- 1	13,68		
92	15	975	60	-0,9	17,1	0,40	30
93	15	970	96	-2,5	17,1	0,35	40
88	25	899	63	-3,2	28,5	0,38	57
89	25	930	54	-4,4	28,5	0,43	45
90	40	844	94	-13,4	45,6	0,35	120
91	40	830	96	-15,8	45,6	0,37	110
94	55	794	101	-16,2	62,7	0,33	191
95	55	799	97	-20	62,7	0,39	143
96	65	778	112	-21	74,1	0,32	253
97	65	770	101	-22,8	74,1	0,36	206
100	80	747	103	-15,8	91,2	0,36	233
101	80	748	112	-21	91,2	0,32	312
99	100	716	100	-19	114	0,36	302
98	100	686	84	-12,2	114	0,39	238

TABLE 1 - Burst data for 1 K/s heating rate

Specimen N°	Burst Pressure (Bar)	Burst Temp. (°C)	Burst Strain (%)	Axial Strain (%)	Initial Stress (MPa)	Maximum Wall Thickness (mm)	Stress at Instability (MPa)
127	3	1210	80	-0,58	3,42		
128	3,5	1215	74		3,99		
69	4	1109	70	-1,6	4,56	0,39	8,5
68	4	1103	83	- 2	4,56	0,36	10
67	5	1061	107	- 3	5,7	0,31	17
60	6	1063	96	-0,7	6,84	0,31	20
65	8	1041	88	-2,6	9,12	0,36	20
64	8	1049	98	-3,2	9,12	0,33	24
61	9	1015	87	-3,2	10,26	0,31	30
63	10	1040	83	-2,8	11,4	0,34	28
62	10	1020	91	- 3	11,4	0,32	32
30	11	1018	80	-2,8	12,3	0,37	26
74	15	990	53	-1,4	17,1	0,42	28
73	20	974	33	-0,8	22,8	0,49	27
84	20	1023	69	-2,4	22,8	0,42	37
72	30	939	49	-2,4	34,2	0,44	51
71	30	940	36	- 2	34,2	0,47	45
87	30	975	43	-2,6	34,2	0,41	59
86	35	918	44	-3,4	39,9	0,46	55
70	45	889	68	-7,8	51,3	0,40	97
85	45	902	80	-11,2	51,3	0,35	131
76	55	848	95		62,7	0,36	132
24	55	840	82	-8,8	62,7	0,34	165
75	55	840	112	-17,4	62,7	0,32	205
77	67	820	94		76,4	0,33	192
78	77	800	96	-15,2	87,8	0,32	280
82	80	837	90	-12,8	91,2	0,35	237
79	85	793	98	-15,8	96,9	0,32	312
81	100	799	89	-14	114	0,36	285
80	116	766	65	-9,2	132,2	0,38	280
83	120	787	66	-9,2	136,8		
18	130	740	68	-7,6	142,6	0,39	295

TABLE 2 - Burst data for 7 K/s heating rate

Specimen N°	Burst Pressure (Bar)	Burst Temp. (°C)	Burst Strain (%)	Axial Strain (%)	Initial Stress (MPa)	Maximum Wall Thickness (mm)	Stress at Instability (MPa)
59	6	1152	88	-2,4	6,84	0,36	15
120	6	1154	104	-3,3	6,84	0,34	17
121	6	1154	95	-3,2	6,84	0,35	18,5
122	8	1117	105	-5,3	9,12	0,32	26
123	8	1110	92	-2,9	9,12	0,36	20
55	10	1025	62	- 1	11,4	0,45	16
43	10	1036	83	- 2	11,4	0,43	18
44	10	1026	53	0	11,4	0,44	17
42	10	1012	46	-0,2	11,4	0,46	15
45	13	1000	54	-1,2	14,8	0,47	19
41	13	967	38	-0,4	14,8	0,47	19
46	15	1018	37	-0,4	17,1		
48	20	963	33,5	-0,5	22,8	0,52	24
47	20	949	26	-0,2	22,8	0,53	23
58	20	939	32	-0,8	22,8	0,48	28
49	22	984	27	-0,3	25	0,52	26
50	23	983	26	-0,6	26,2	0,52	27
51	25	995	32	-0,6	28,5	0,50	32
52	30	937	20	-0,6	34,2	0,49	39
57	30	917	29	- 1	34,2	0,48	42
56	45	903	47	- 4	51,3	0,41	98
54	45	910	41	-3,3	51,3	0,44	77
53	45	904	34	-3,2	51,3	0,48	65
119	70	875	92	-14,4	79,8	0,39	171
118	80	893	85	-9,7	91,2	0,39	186
117	80	890	70	-11,2	91,2	0,38	198
116	90	855	84	-15,3	102,6	0,35	275
115	90	832	70	-7,3	102,6	0,41	185
114	100	832	66	- 11	114	0,41	213
113	100	830	84	-11,4	114	0,37	262
126	125	822	54	-8,6	142,5	0,40	273
125	127	810	66	-9,7	144,8	0,39	294
124	130	794	54	-3,9	148,2	0,44	224

TABLE 3 - Burst data for 15 K/s heating rate

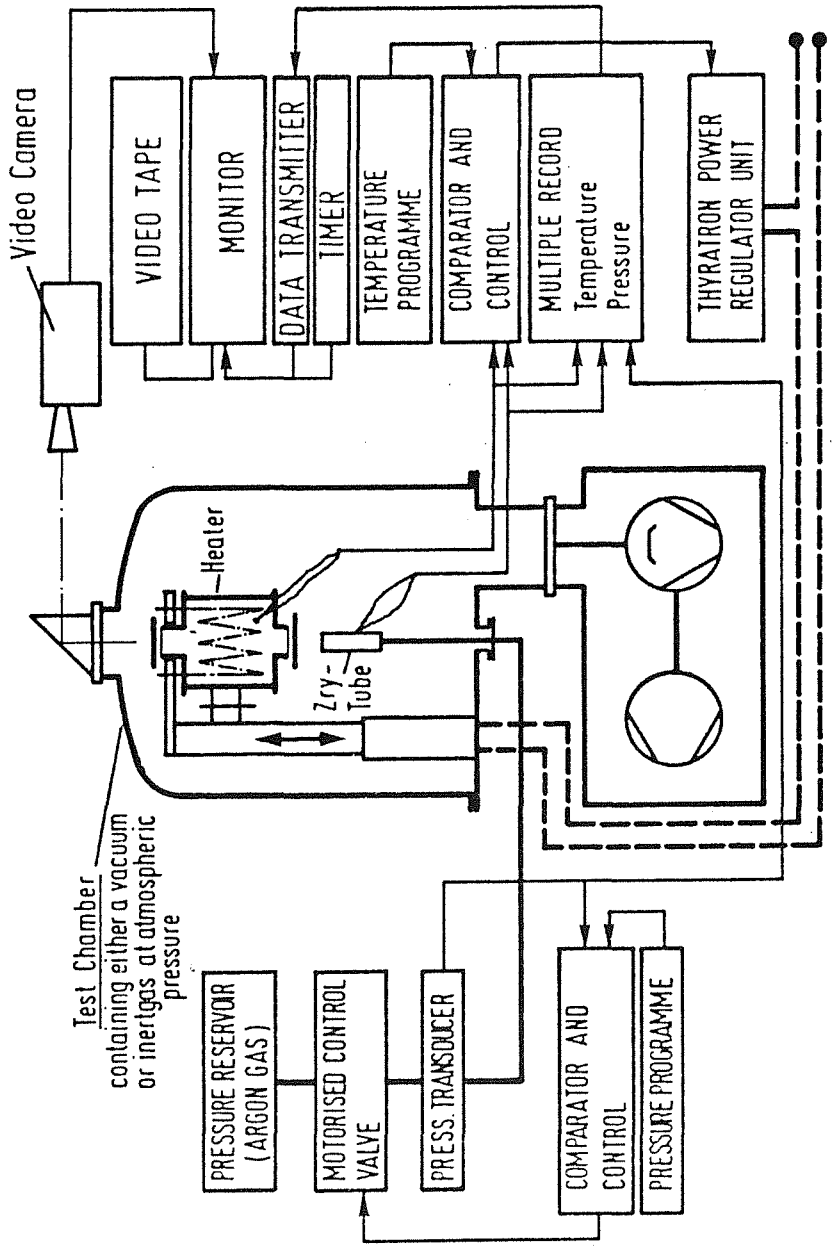

Fig. 1: Diagram of the TUBA test apparatus

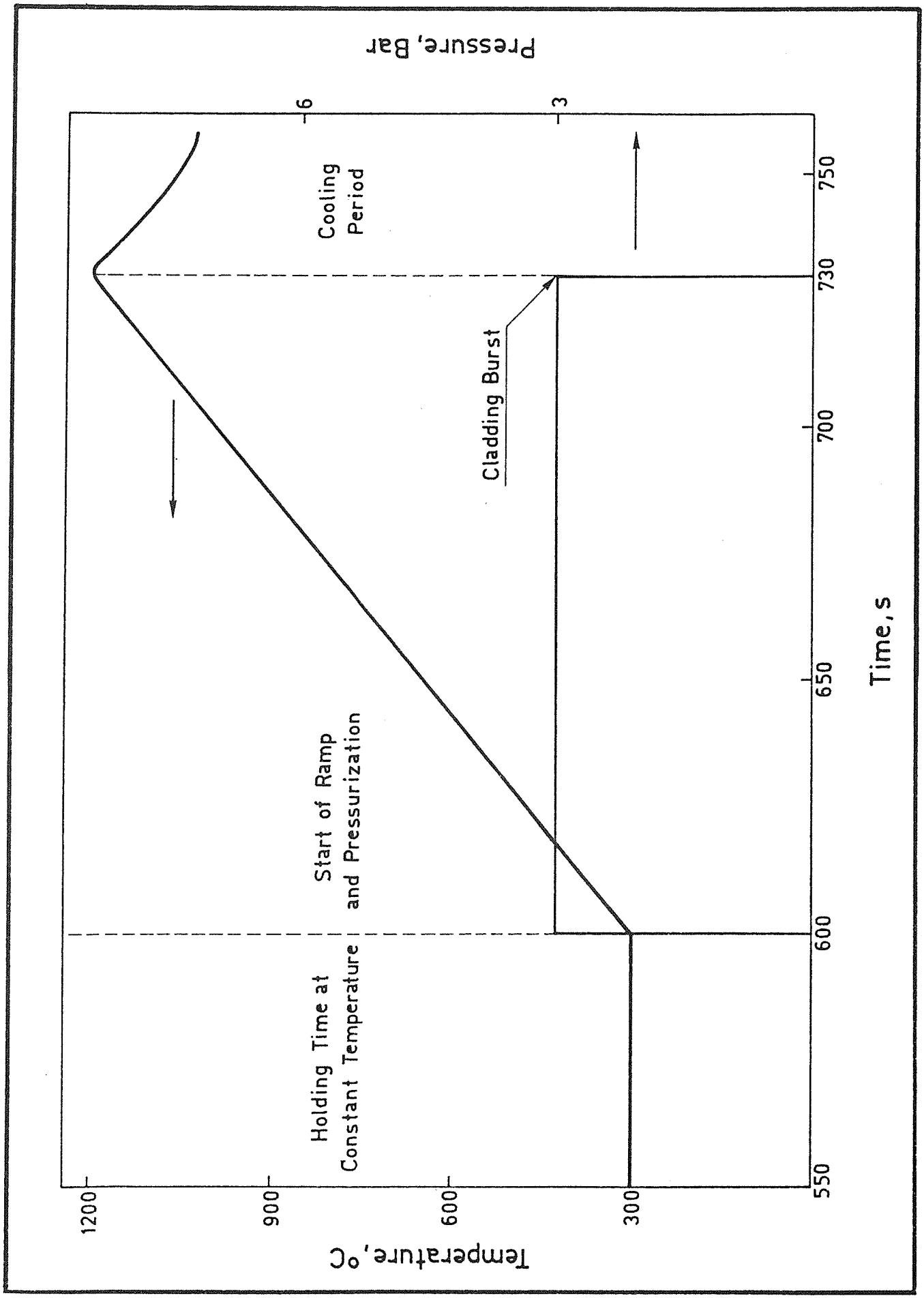

Fig. 2: Typical temperature and pressure history

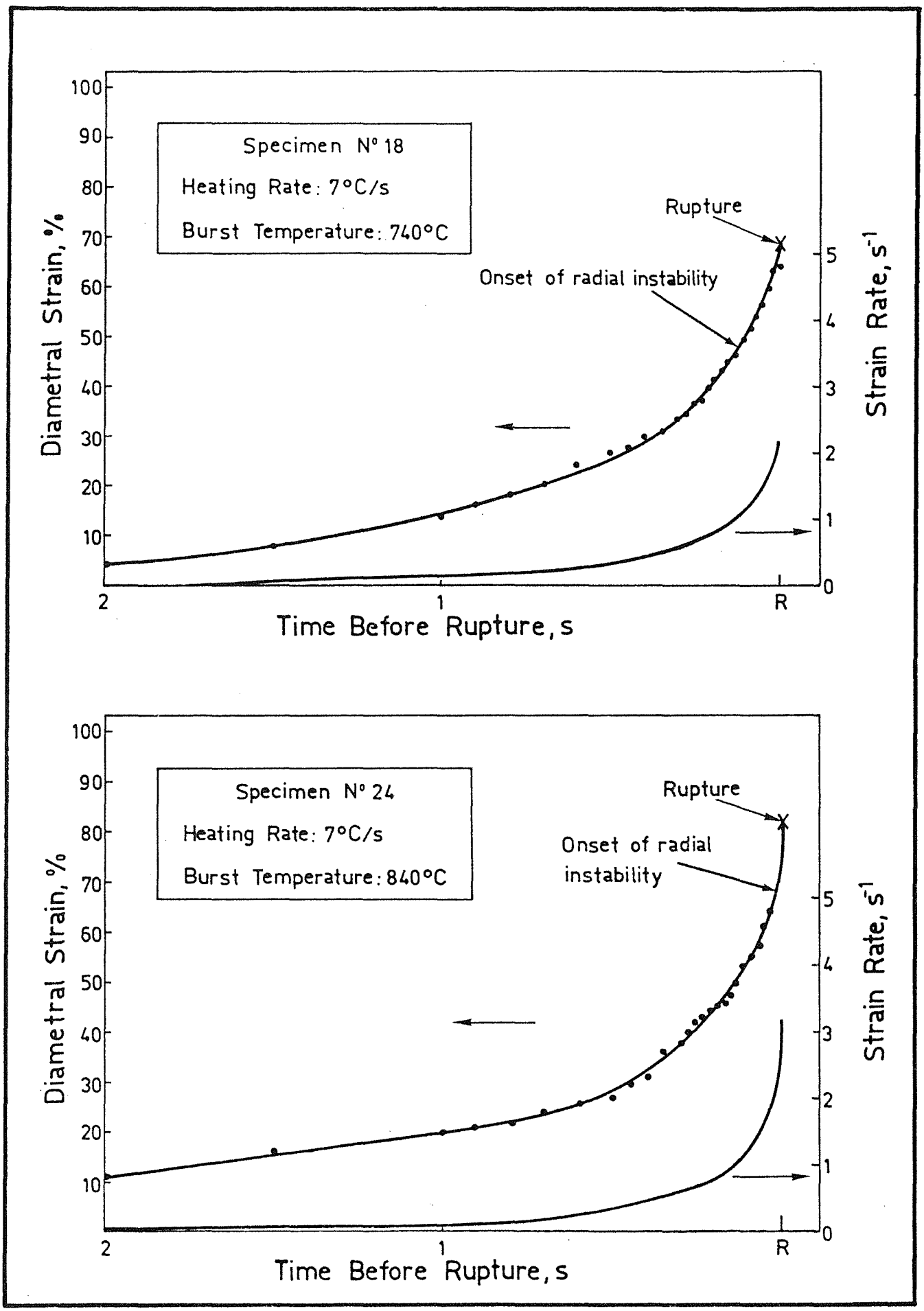

Fig. 3: Circumferential strain and strain rate histories versus time

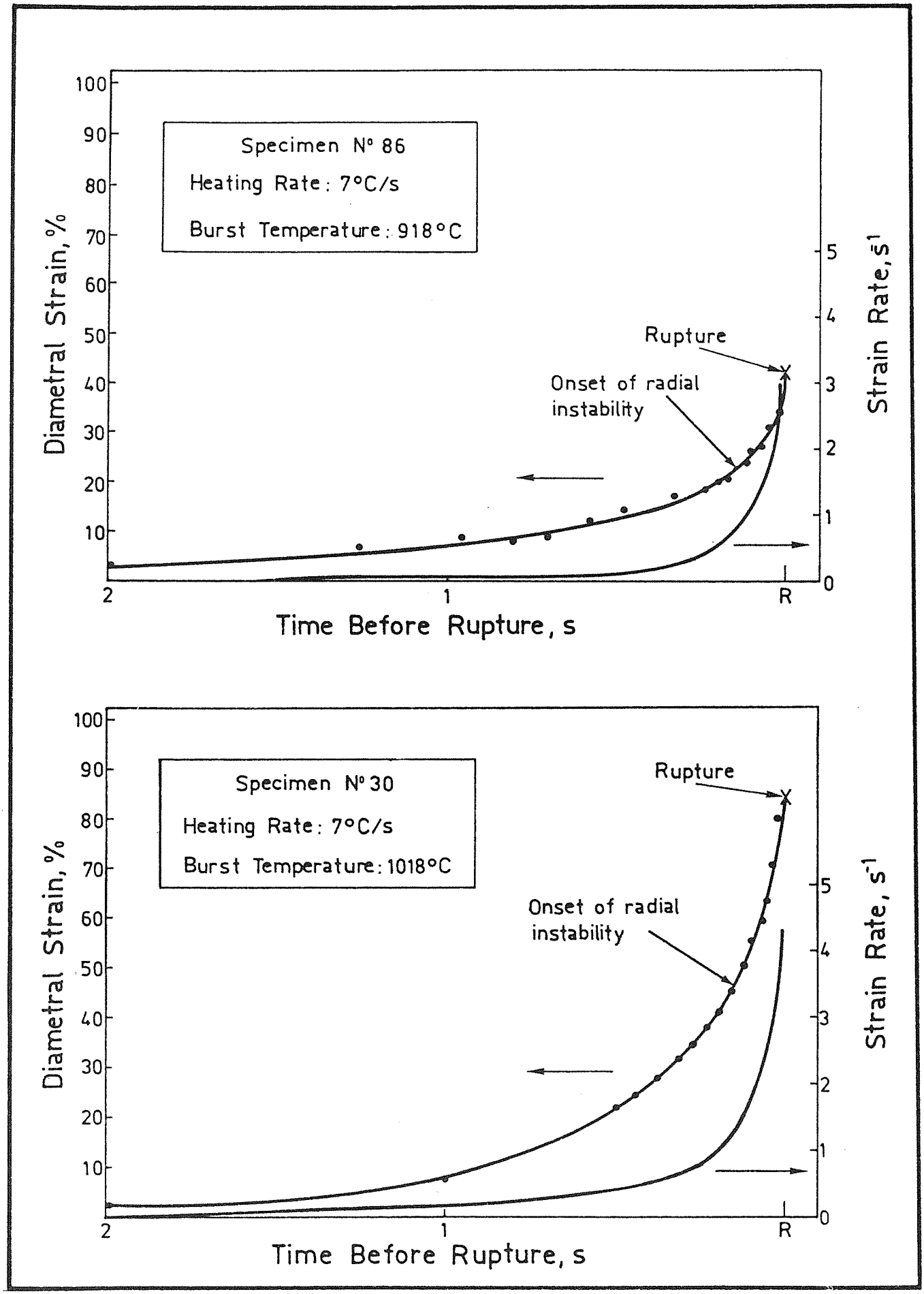

Fig. 4: Circumferential strain and strain rate histories versus time

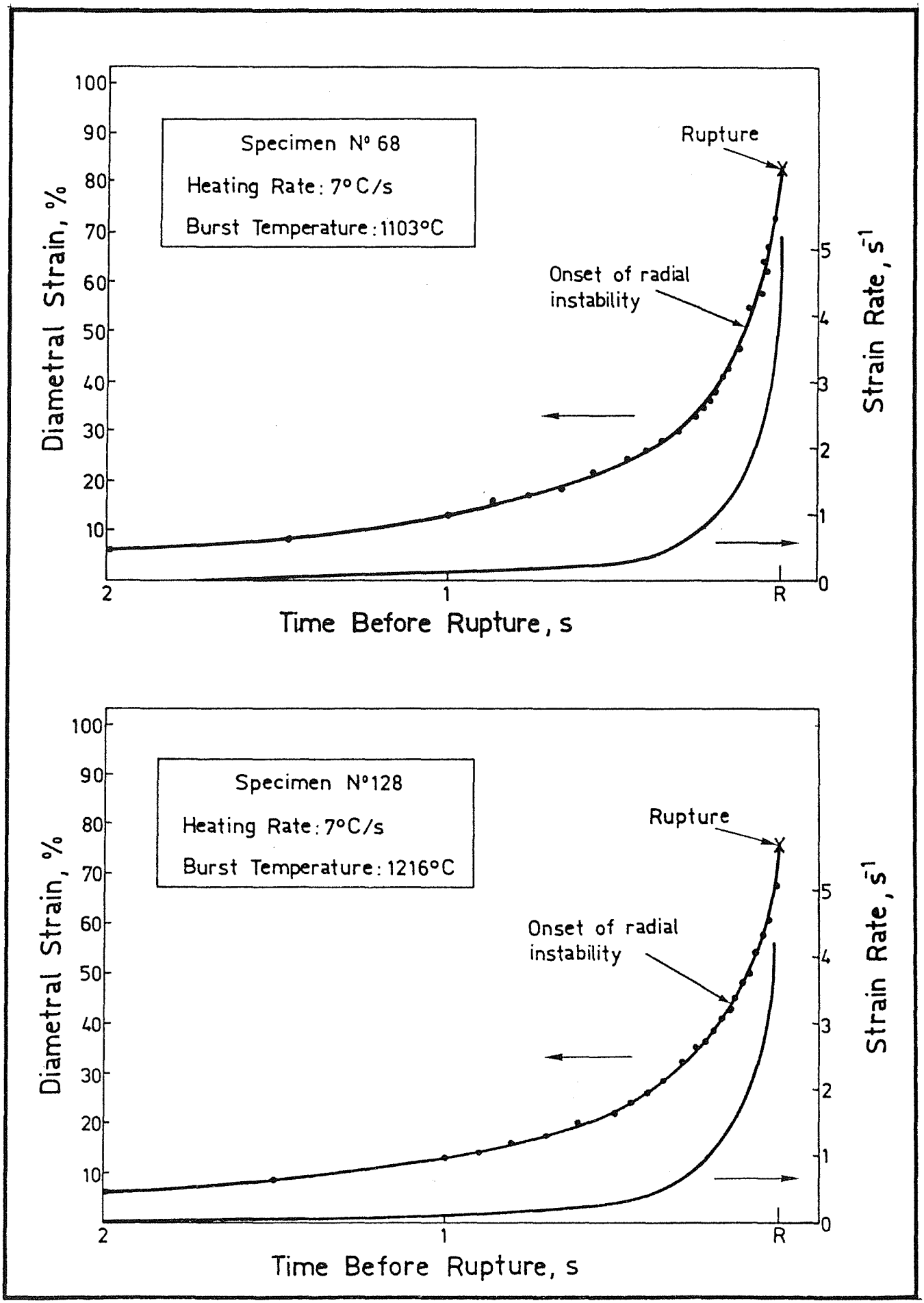

Fig. 5: Circumferential strain and strain rate historiesversus time

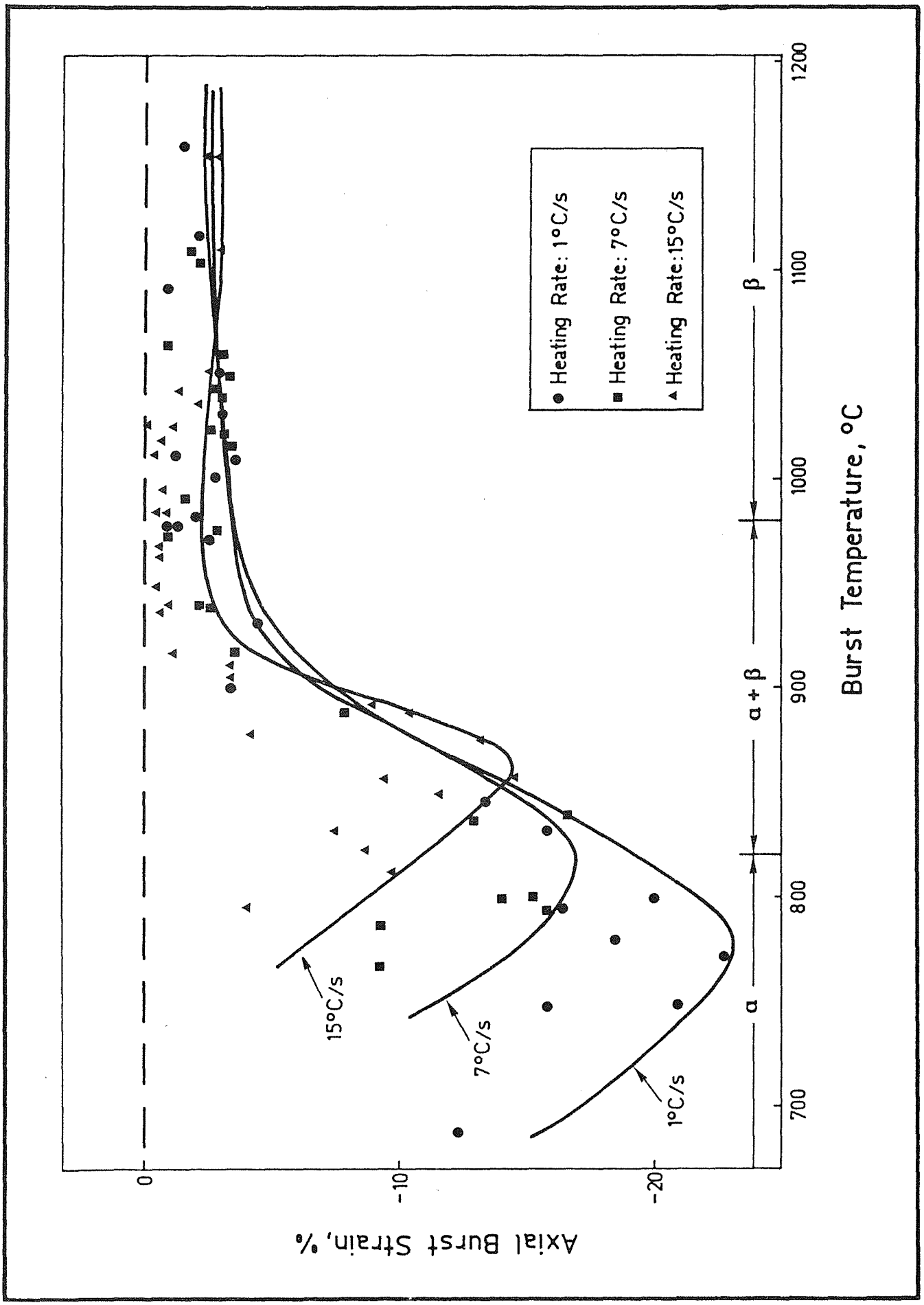

Fig. 6: Change in the axial strain as function of burst temperature

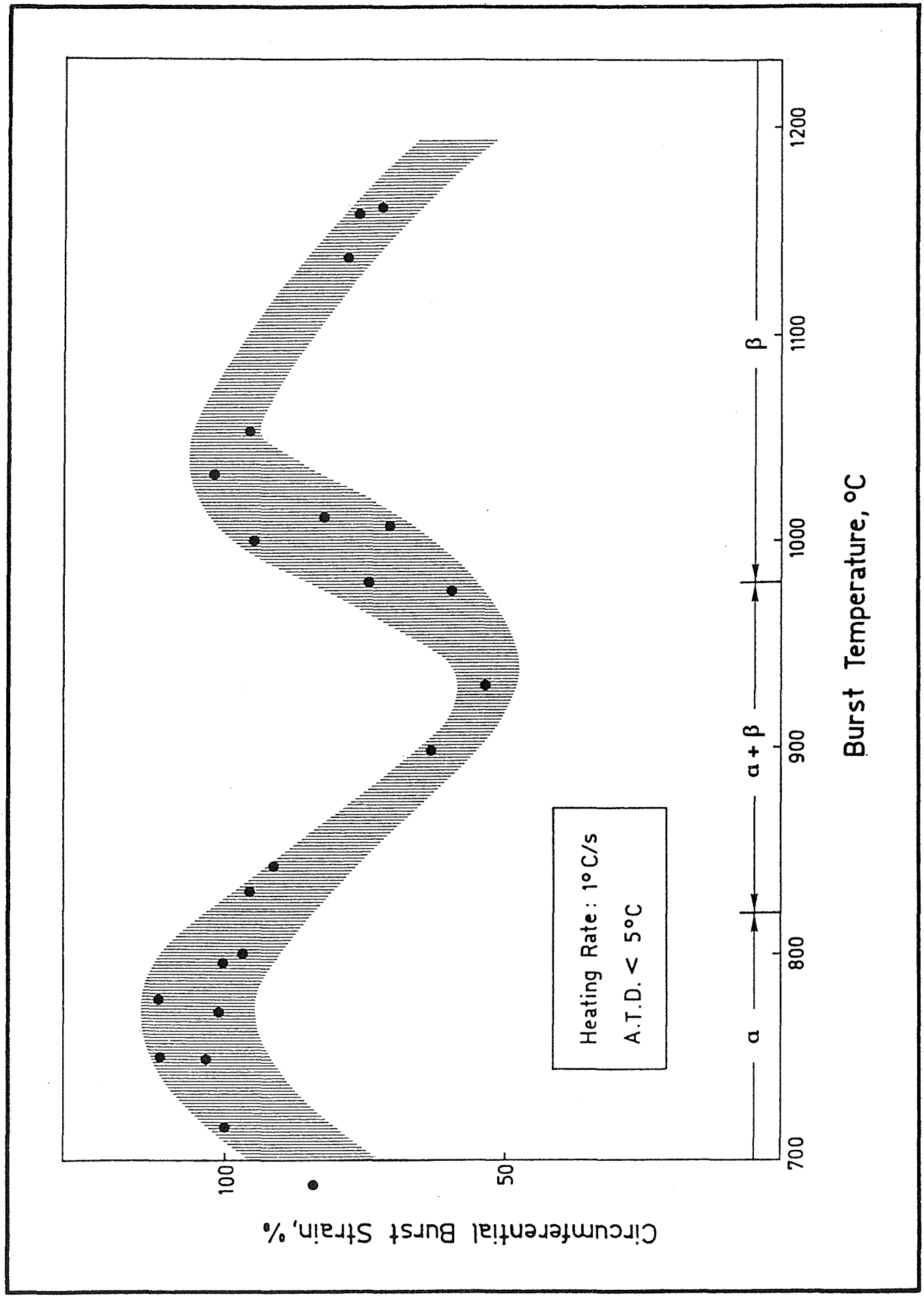

Fig. 7: Circumferential strain versus burst temperature. Specimens heated at 1 K/s

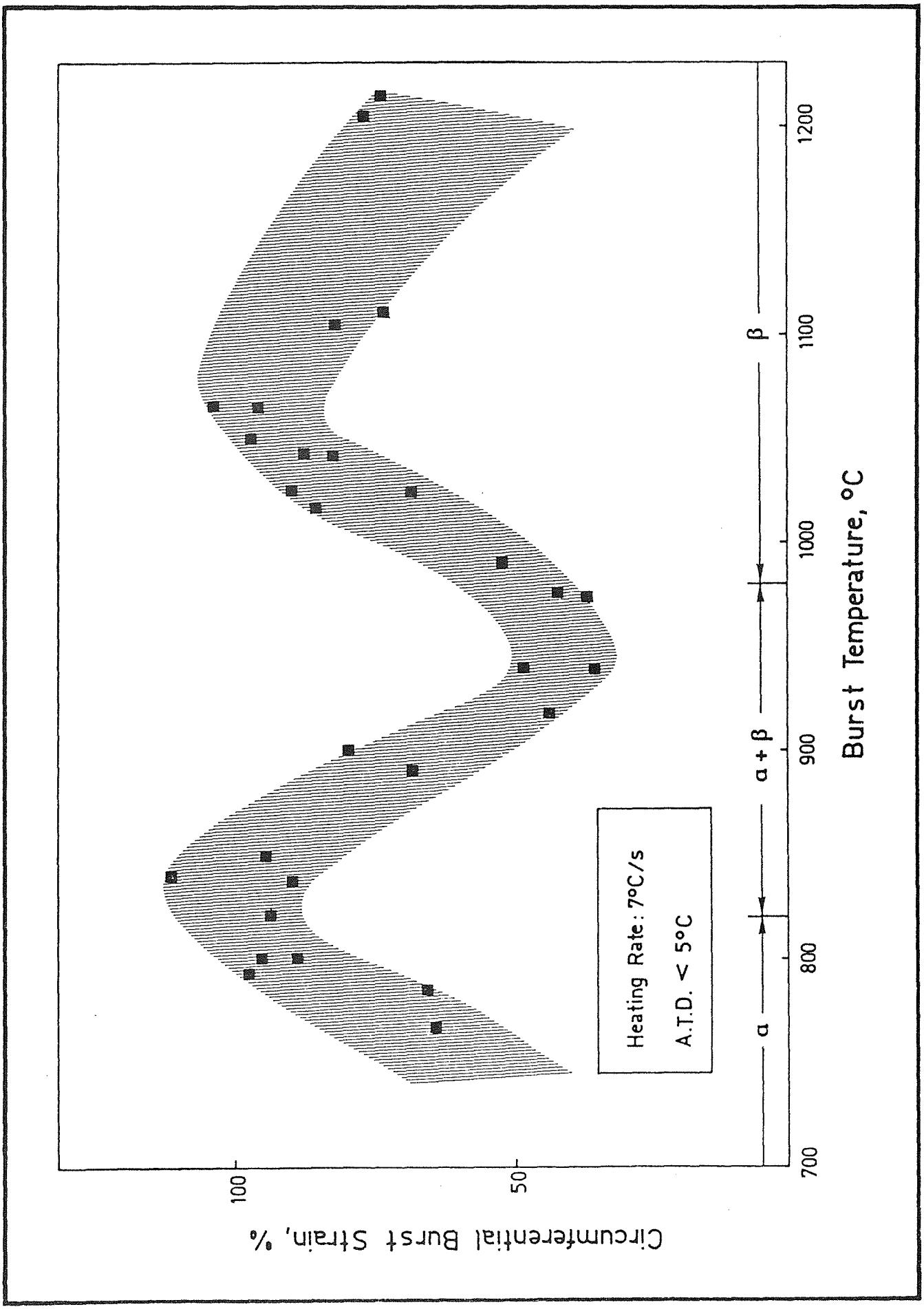

Fig. 8: Circumferential strain versus burst temperature. Specimens heated at 7 K/s

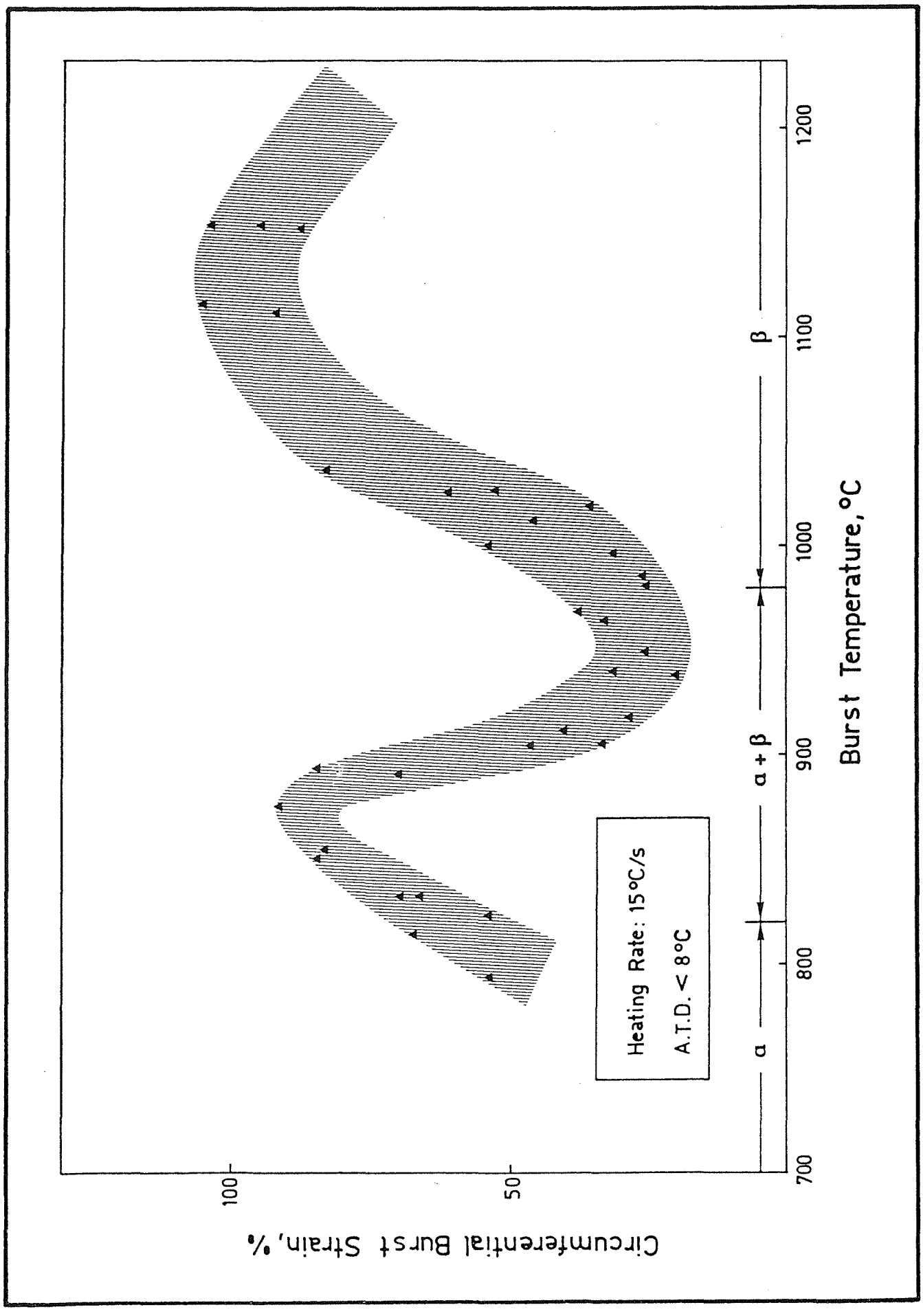

Fig. 9: **Circumferential strain versus burst temperature. Specimens heated at 15 K/s**

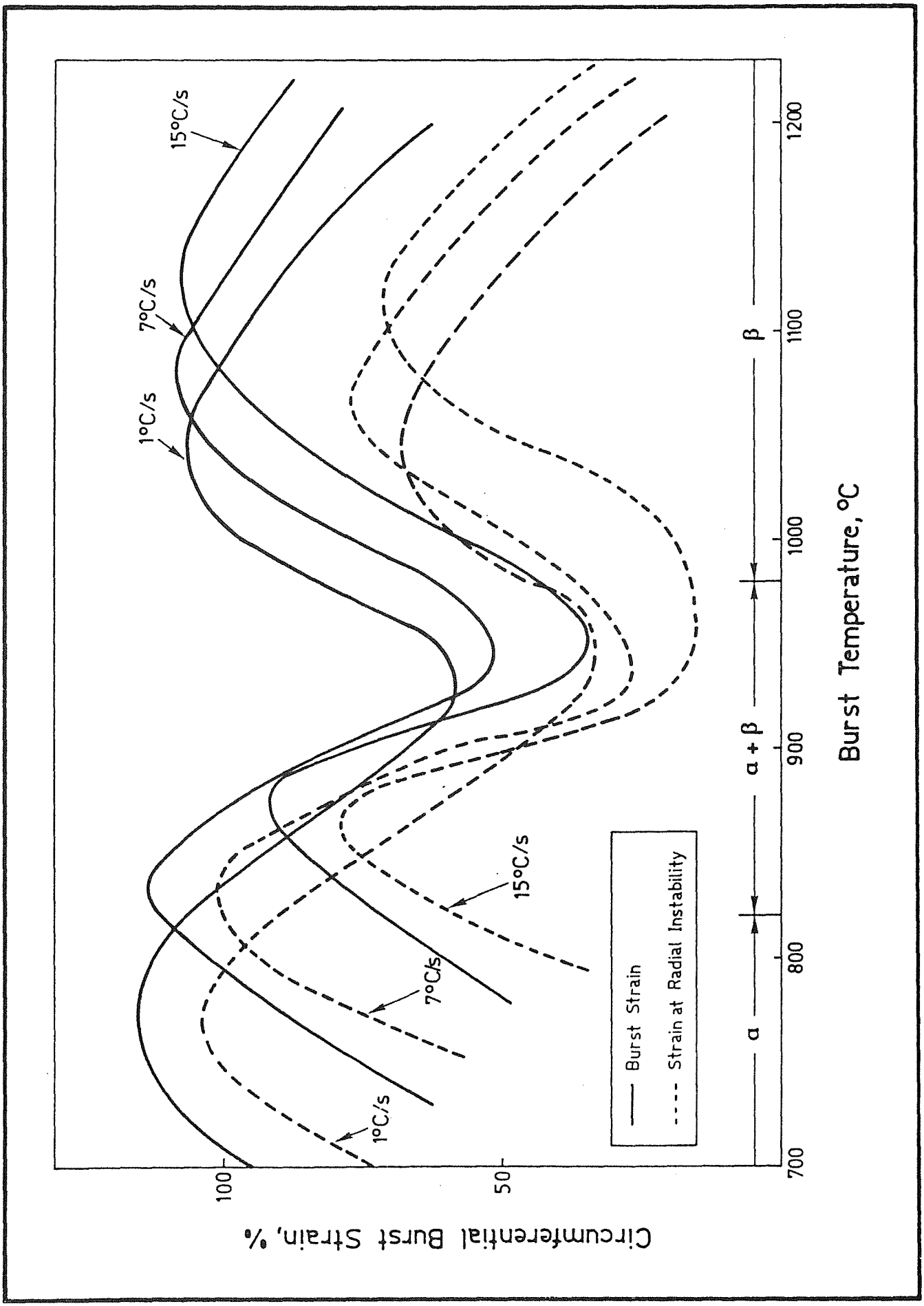

Fig. 10: Circumferential burst and circumferential strain at radial instability

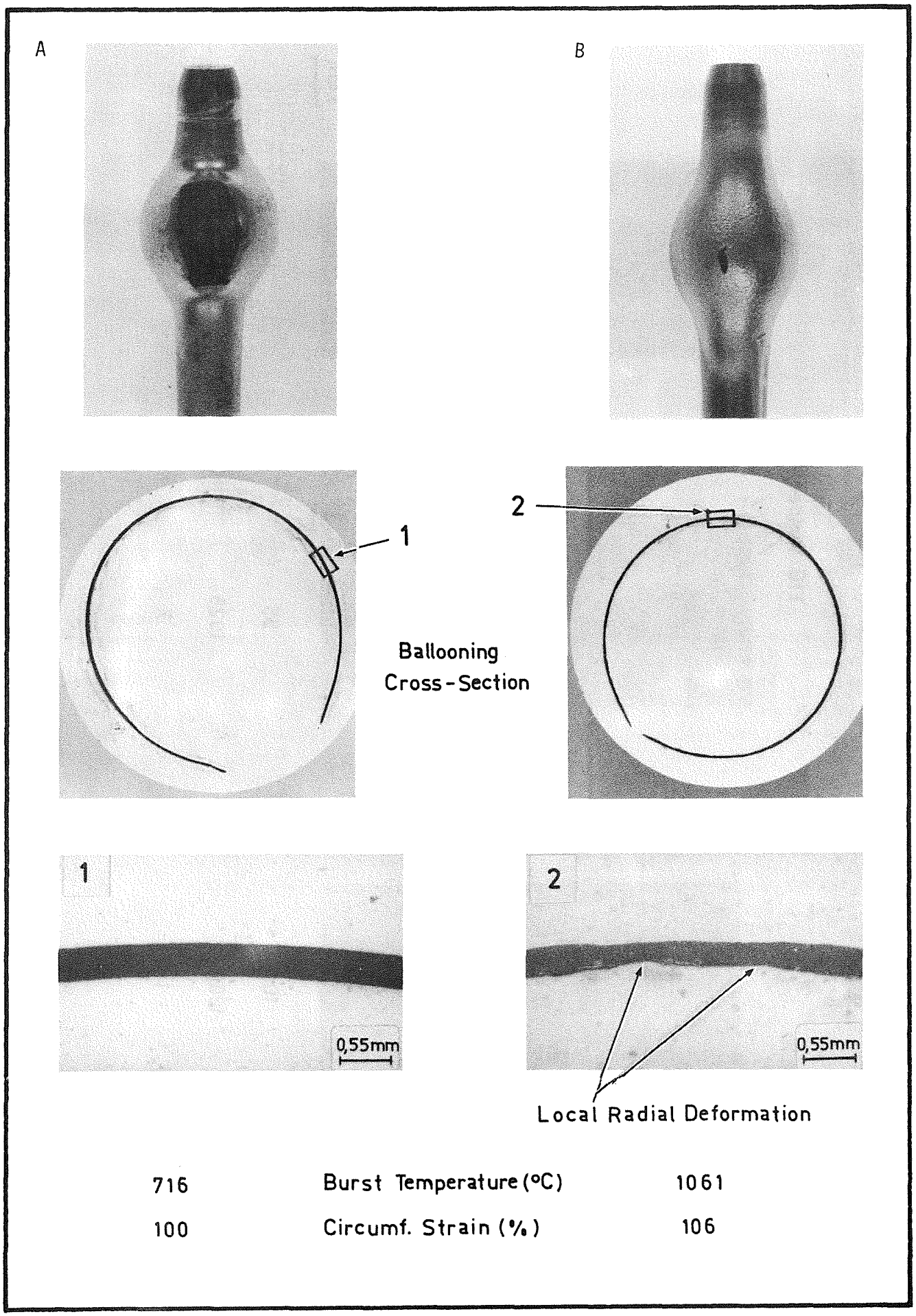

Fig. 11: Longitudinal and rupture cross section view of specimens burst in the α and β-phase, respectively

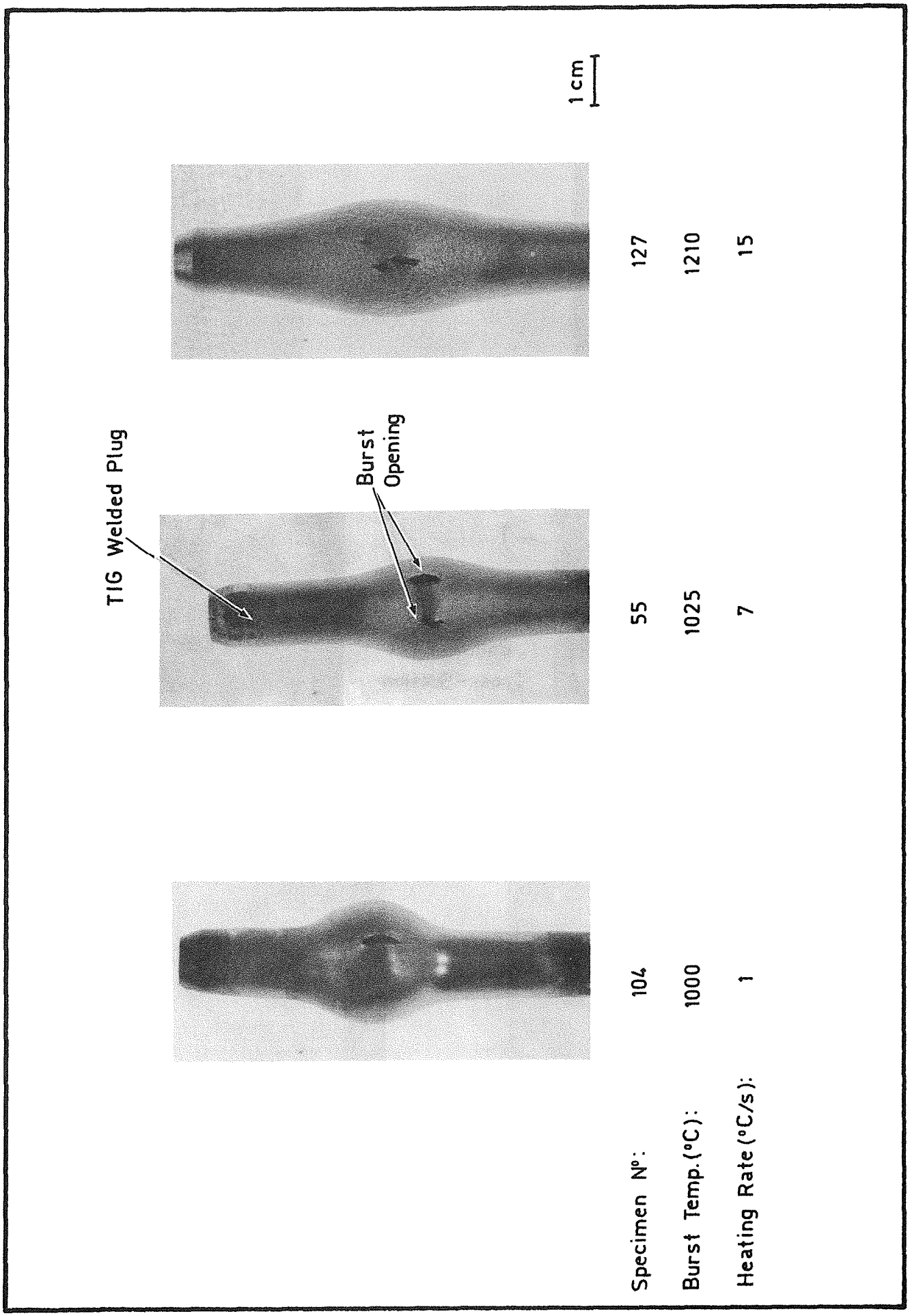

Fig. 12: Specimens failed in the β-phase with more than one burst opening

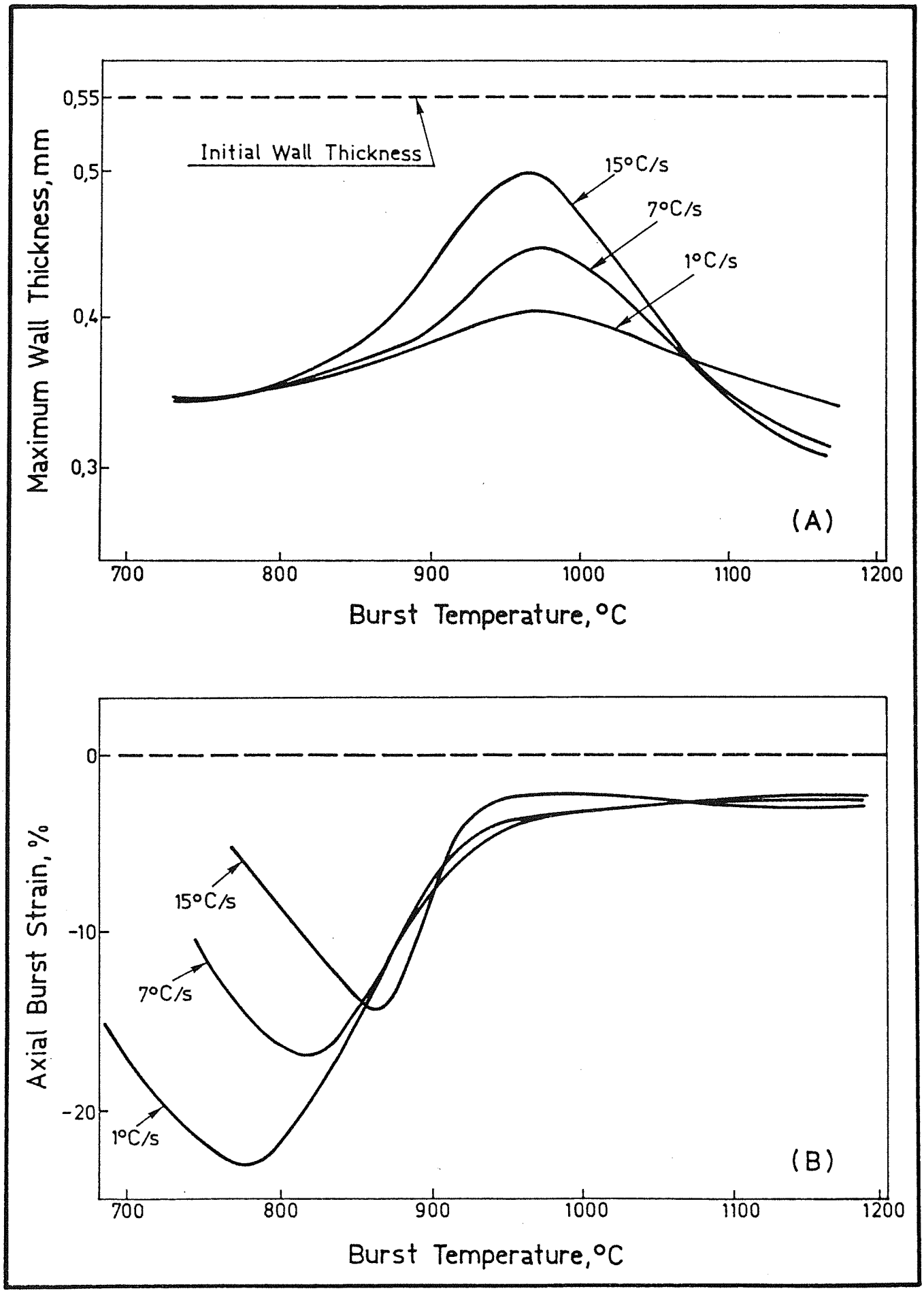

Fig. 13: Maximum wall thickness after burst (A) and axial strain (B), as a function of burst temperature

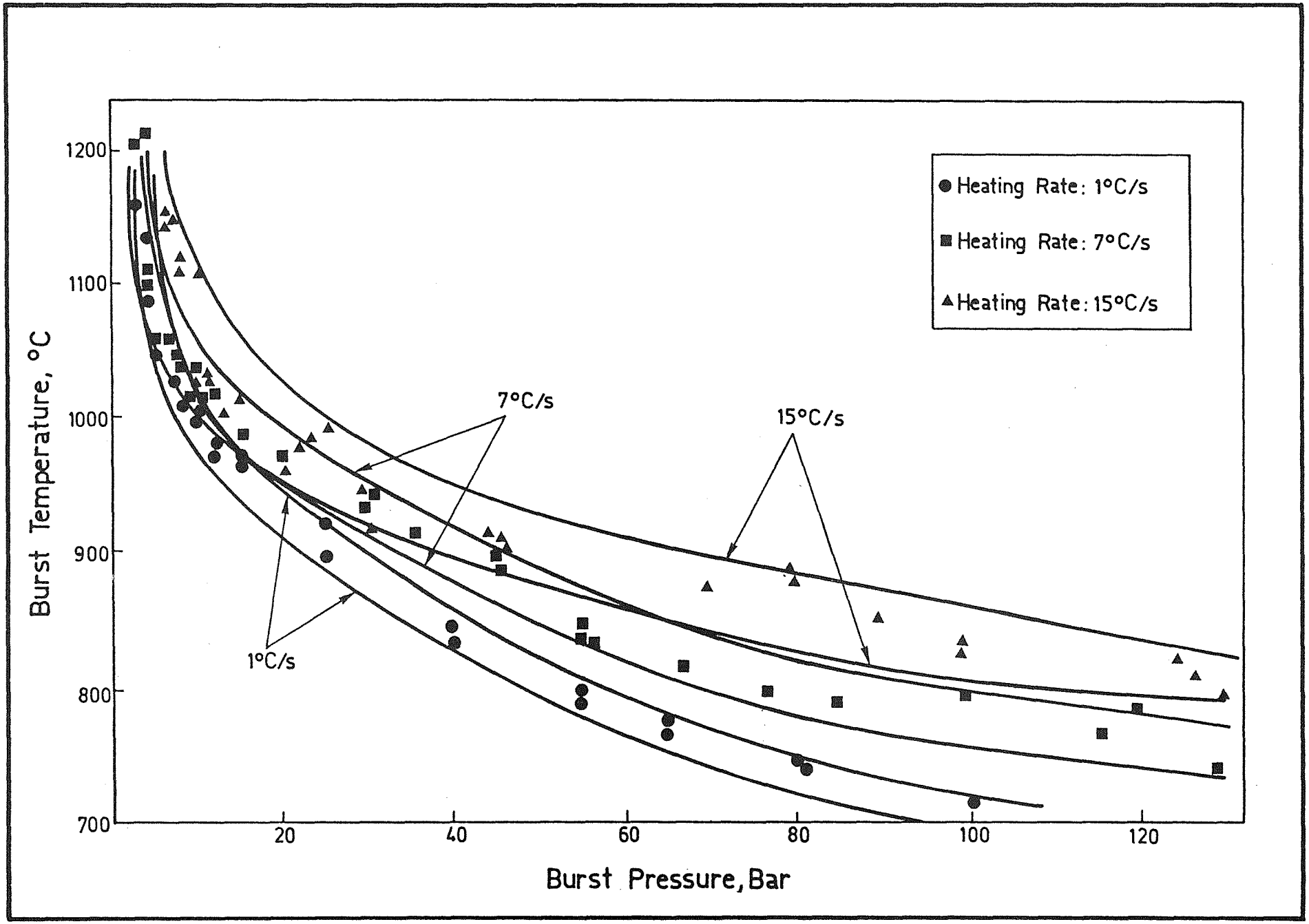

Fig. 14: Dependence of burst temperature on burst pressure

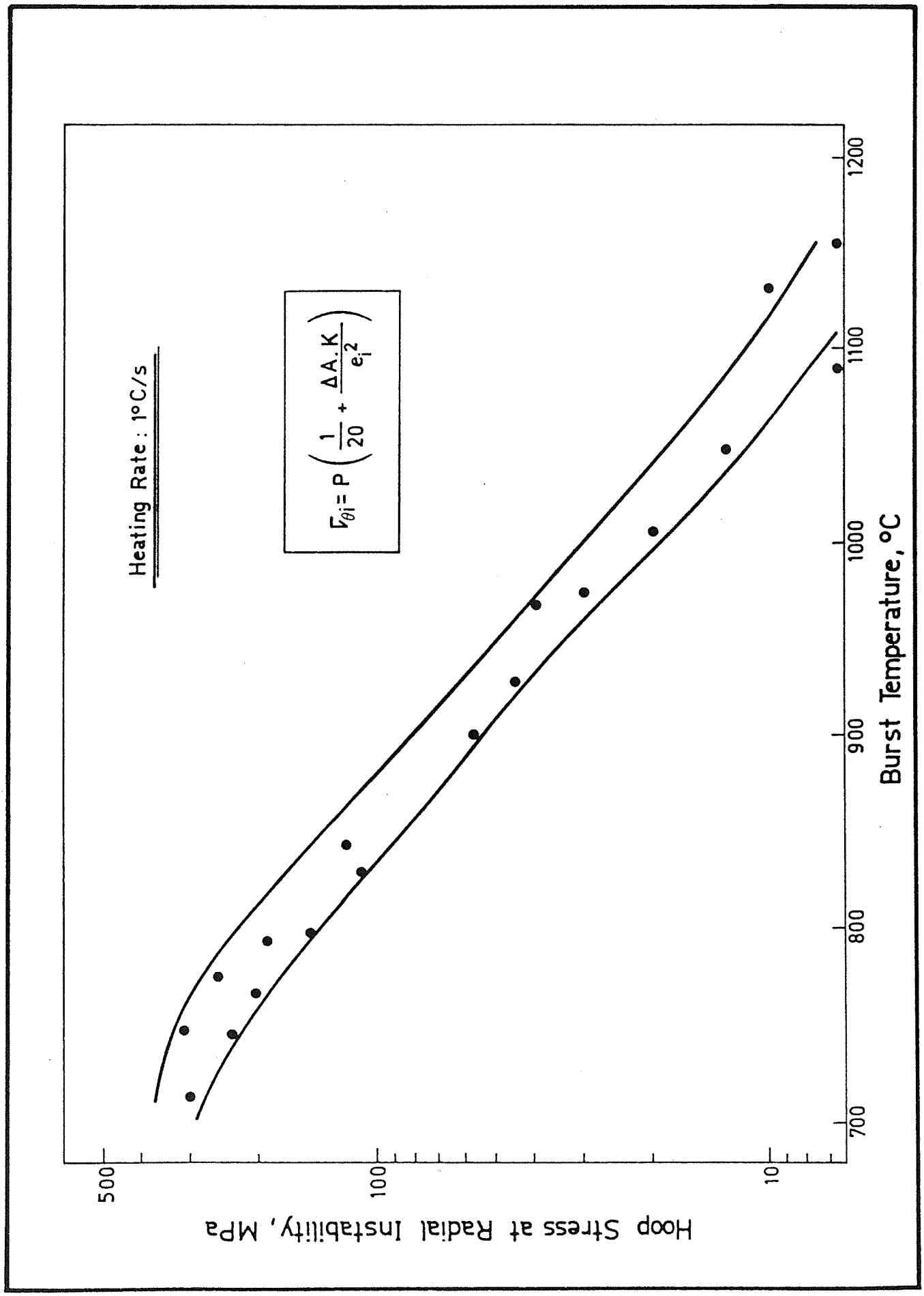

Fig.. 15: Circumferential stress at radial instability versus burst temperature. Specimens heated at 1 K/s

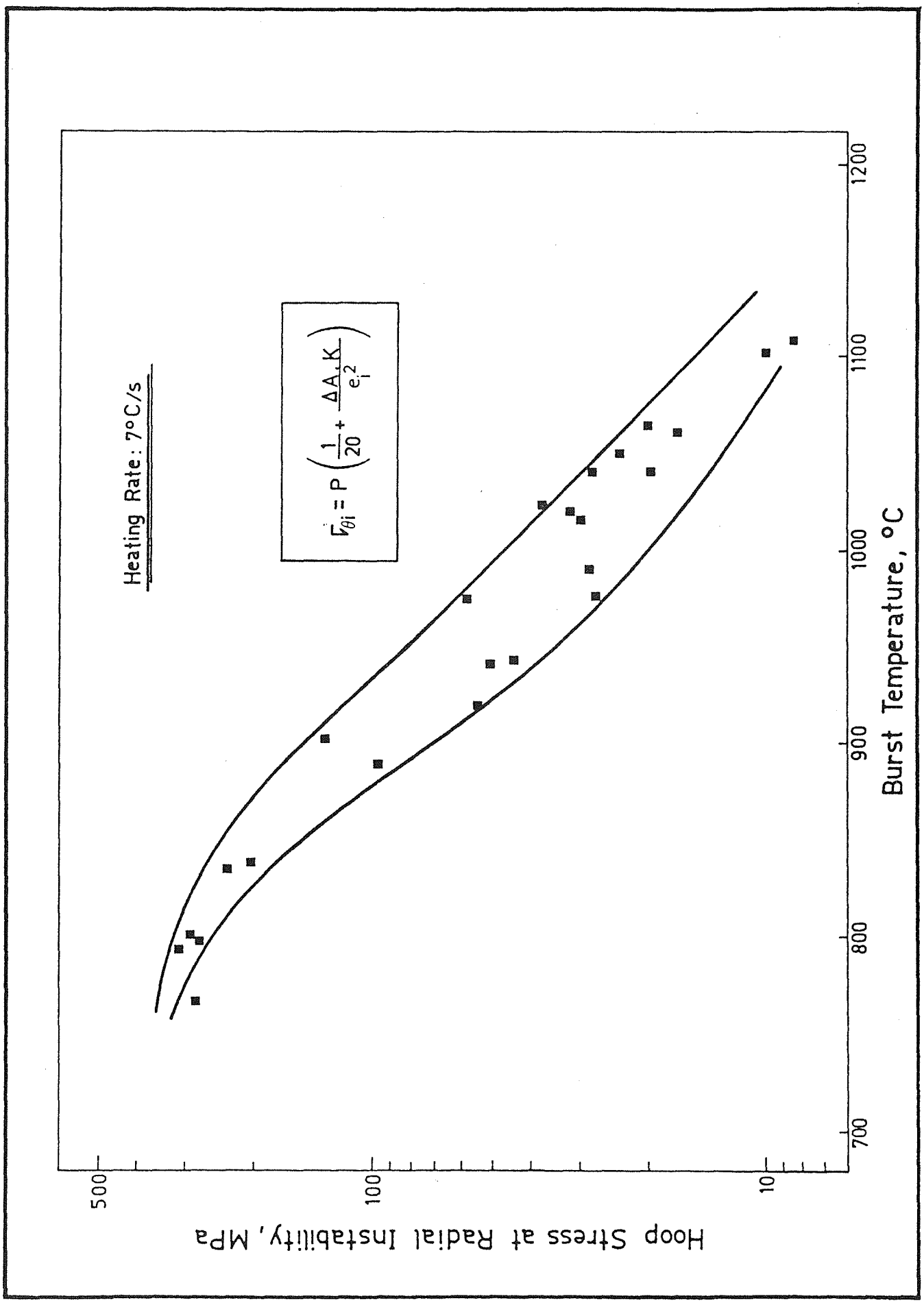

Fig. 16: Circumferential stress at radial instability versus burst temperature. Specimens heated at 7 K/s

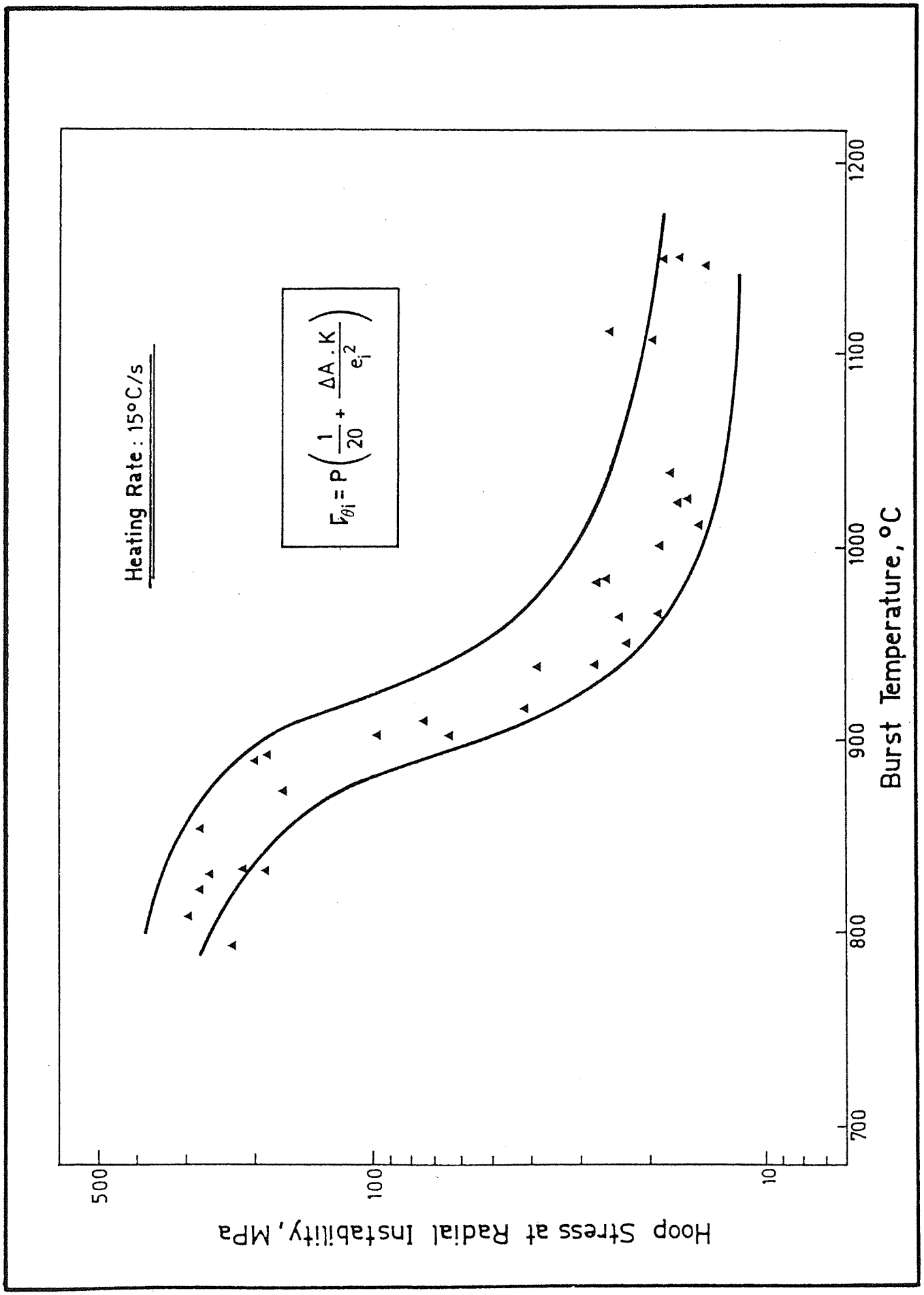

Fig. 17: Circumferential stress at radial instability versus burst temperature. Specimens heated at 15 K/s

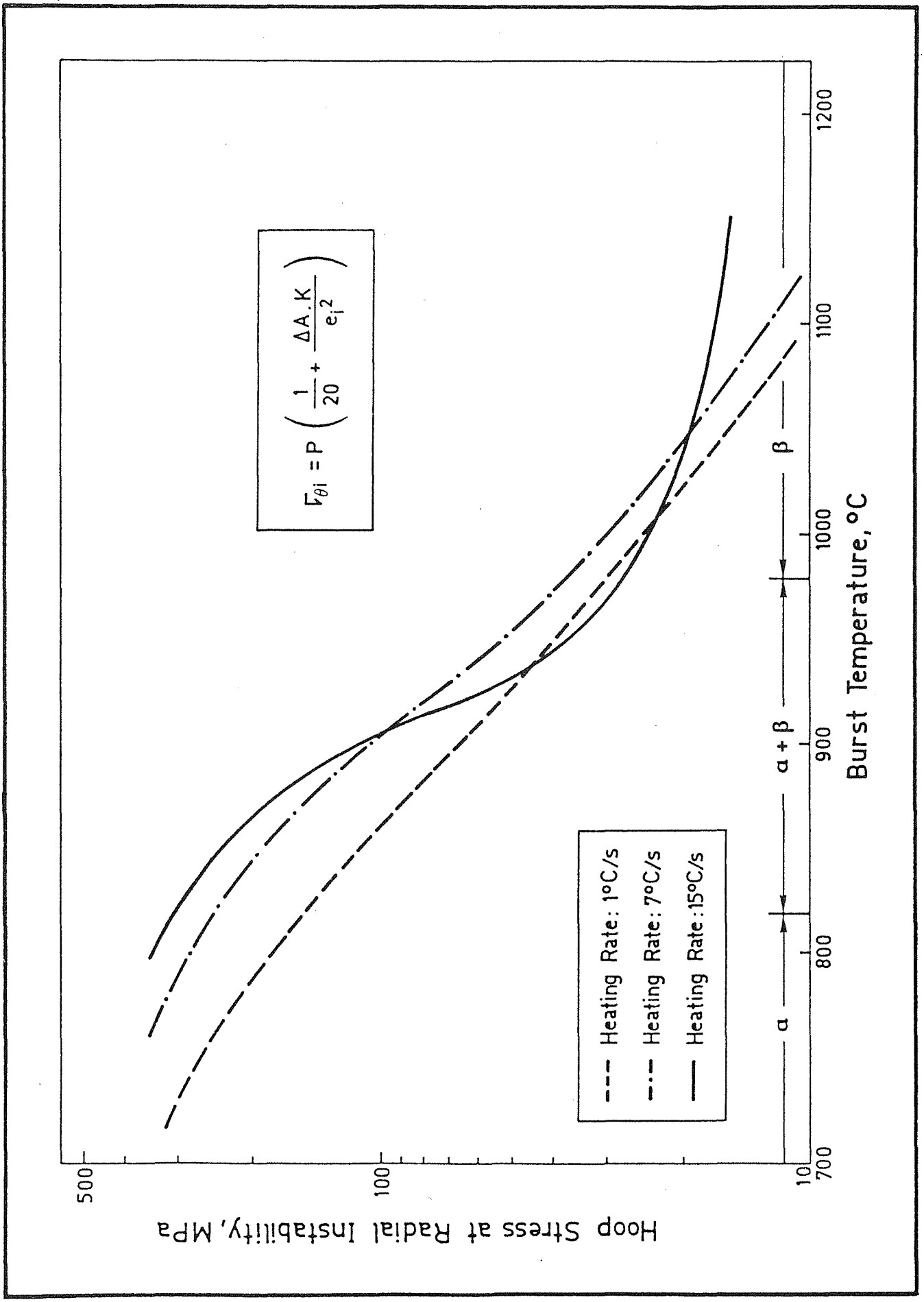

Fig. 18: Comparison of circumferential stress at radial instability for different heating rates

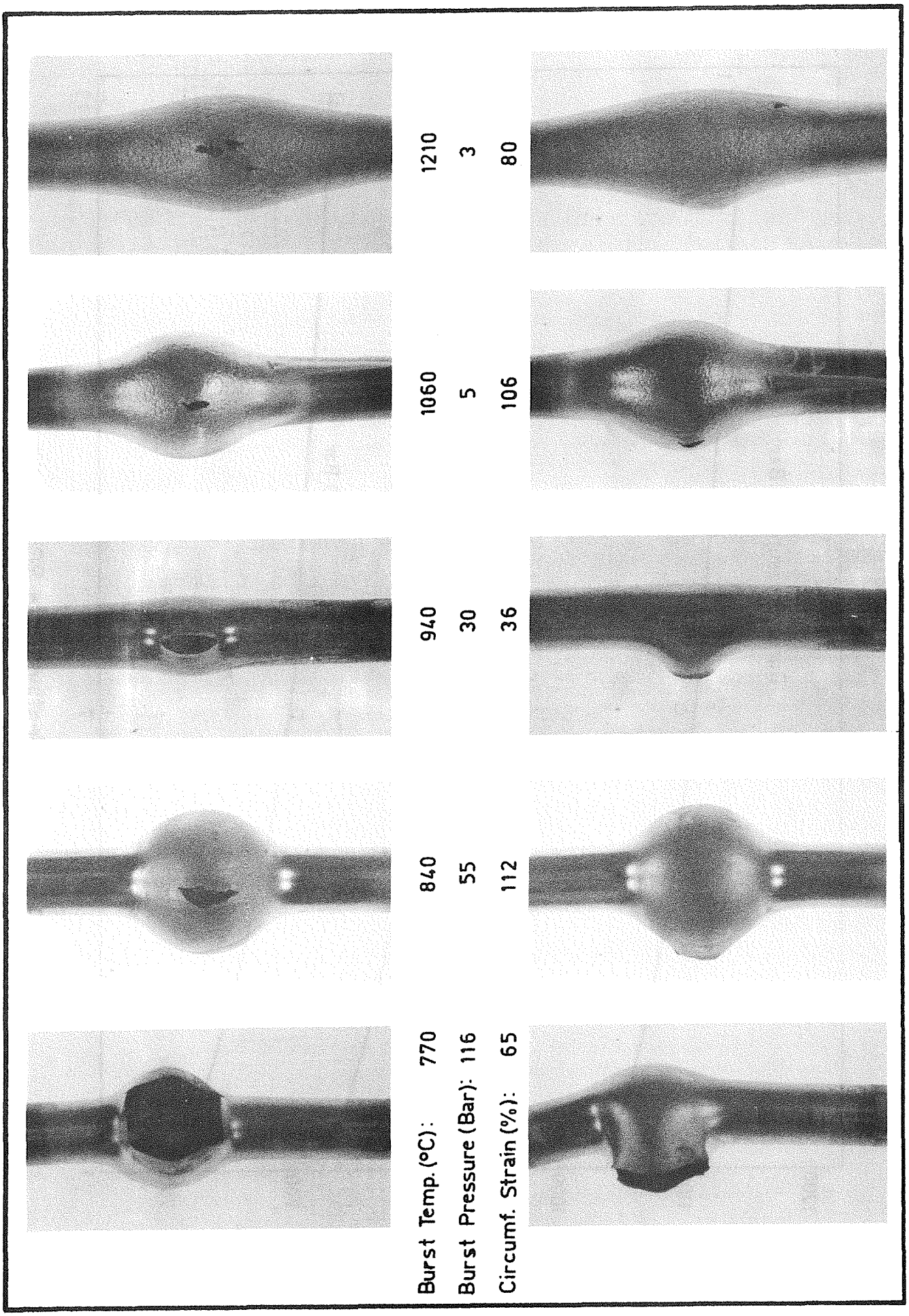

Fig. 19: Typical failure mode at different burst temperature

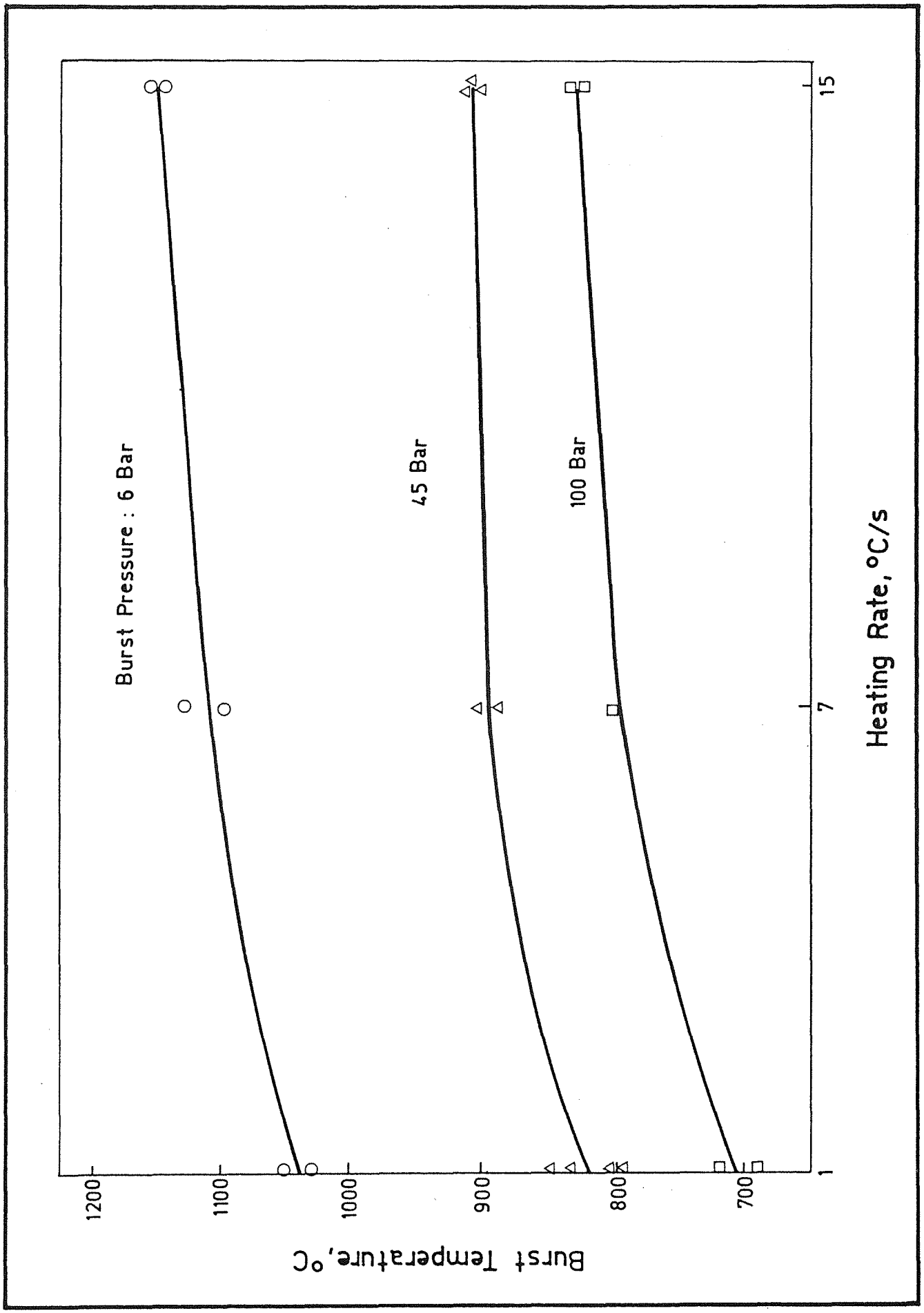

Fig. 20: Effect of heating rate on burst temperature at different internal pressures

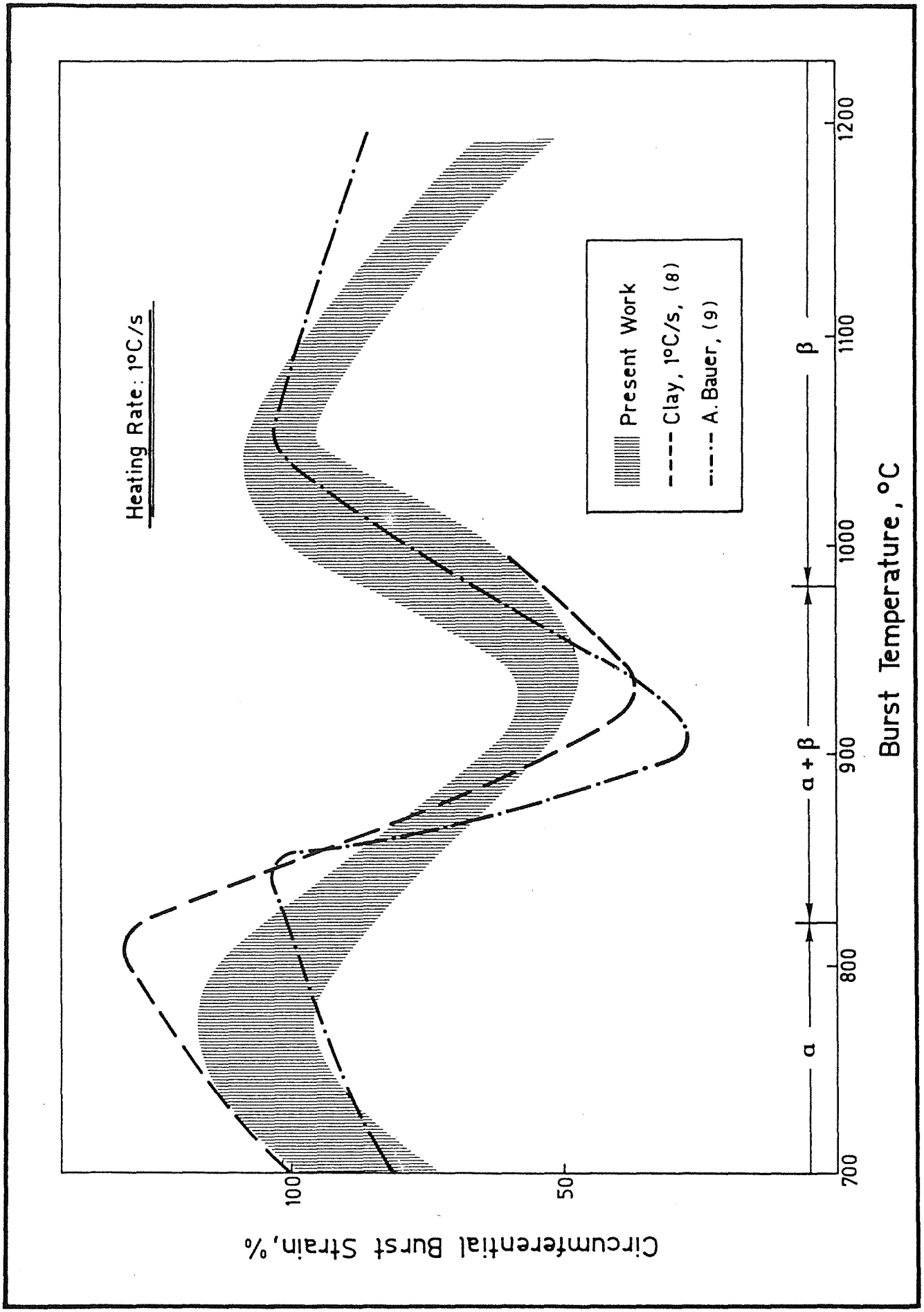

Fig. 21: Comparison of circumferential strain versus burst temperature with other experimental works. Heating rate 1 K/s

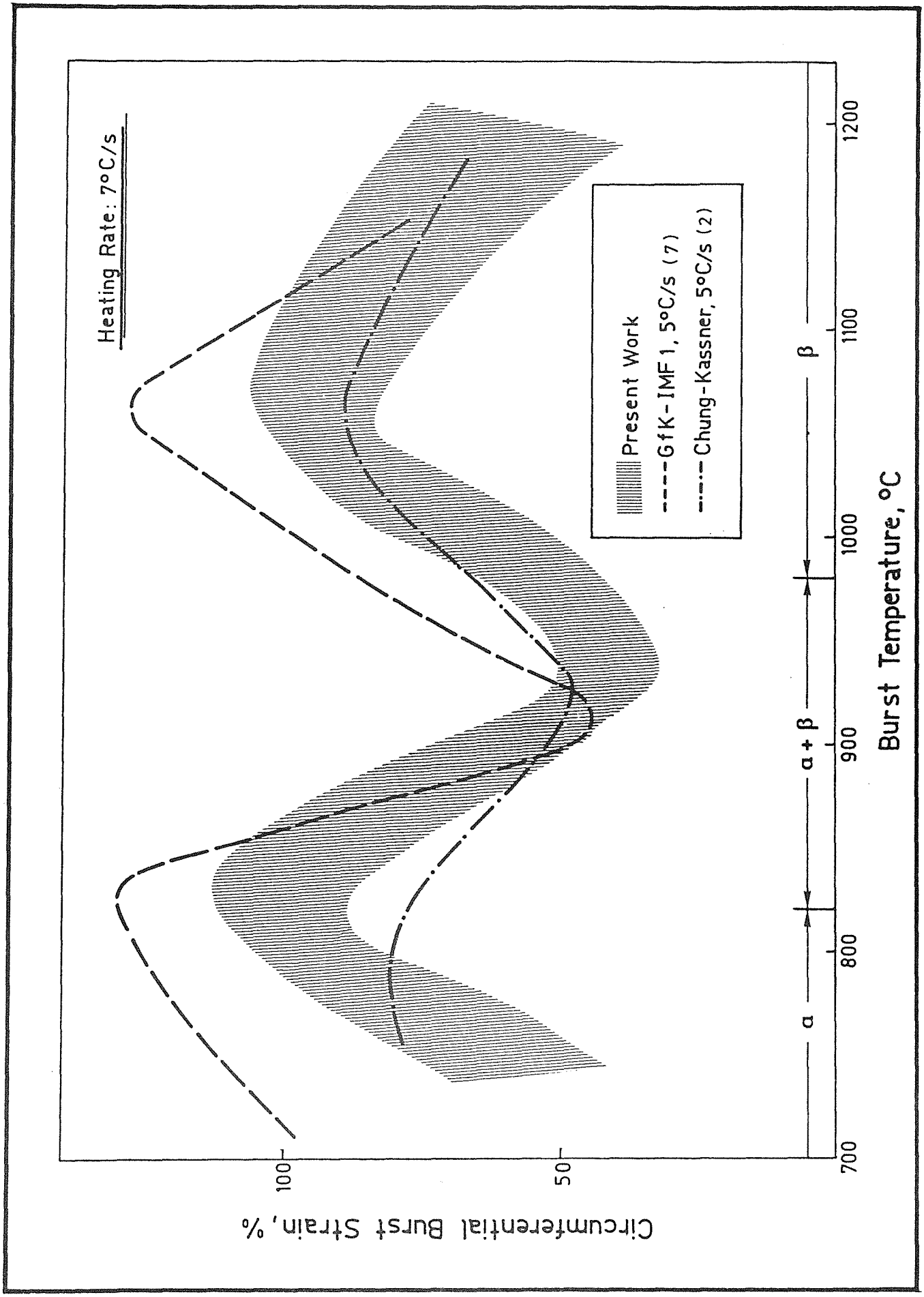

Fig. 22: Comparison of circumferential strain versus burst temperature with other experimental works. Heating rate 7 K/s

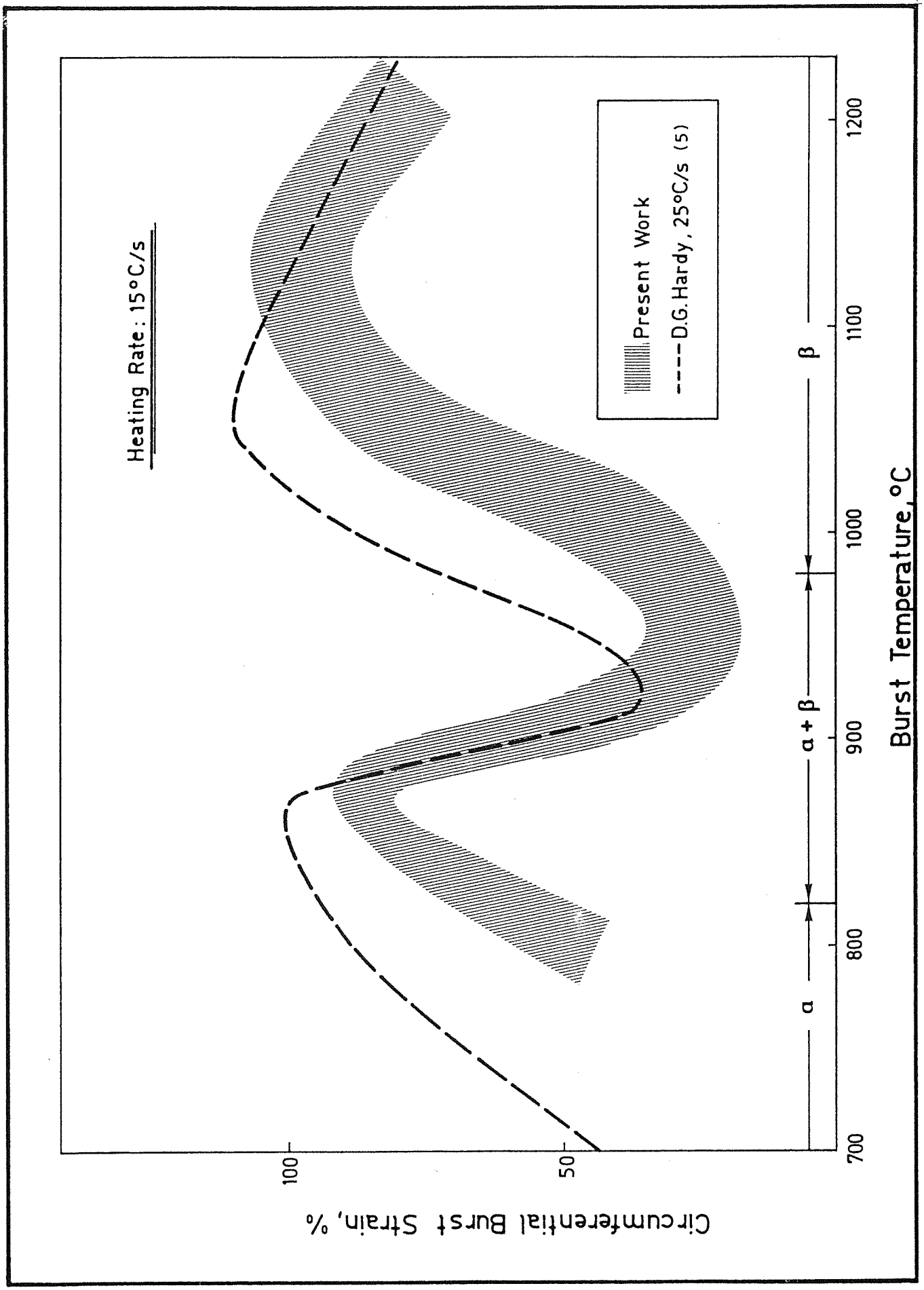

Fig. 23: Comparison of circumferential strain versus burst temperature with other experimental works. Heating rate 15 K/s

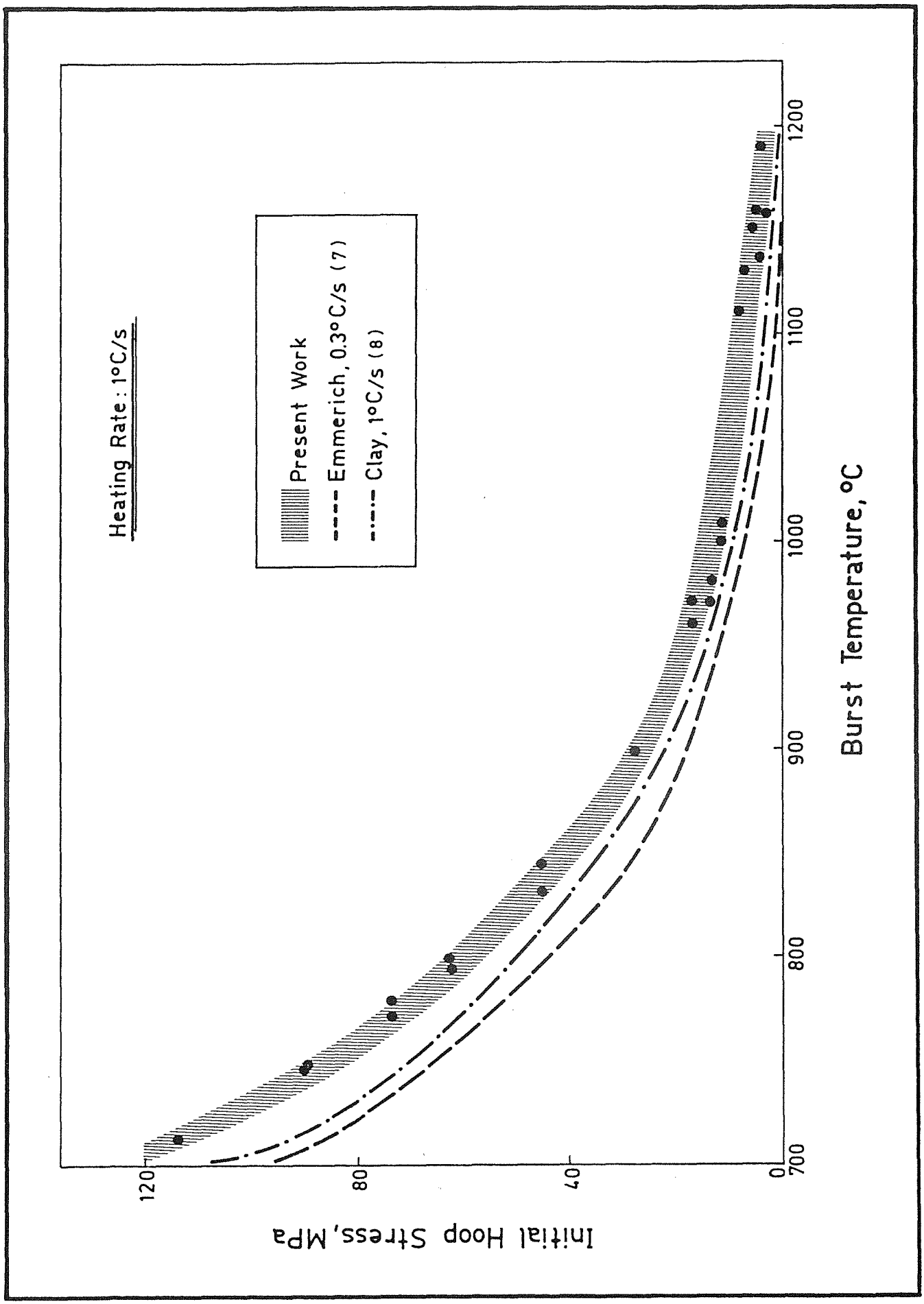

Fig. 24: Comparison of initial hoop stress versus burst temperature with other experimental works. Heating rate 1 K/s

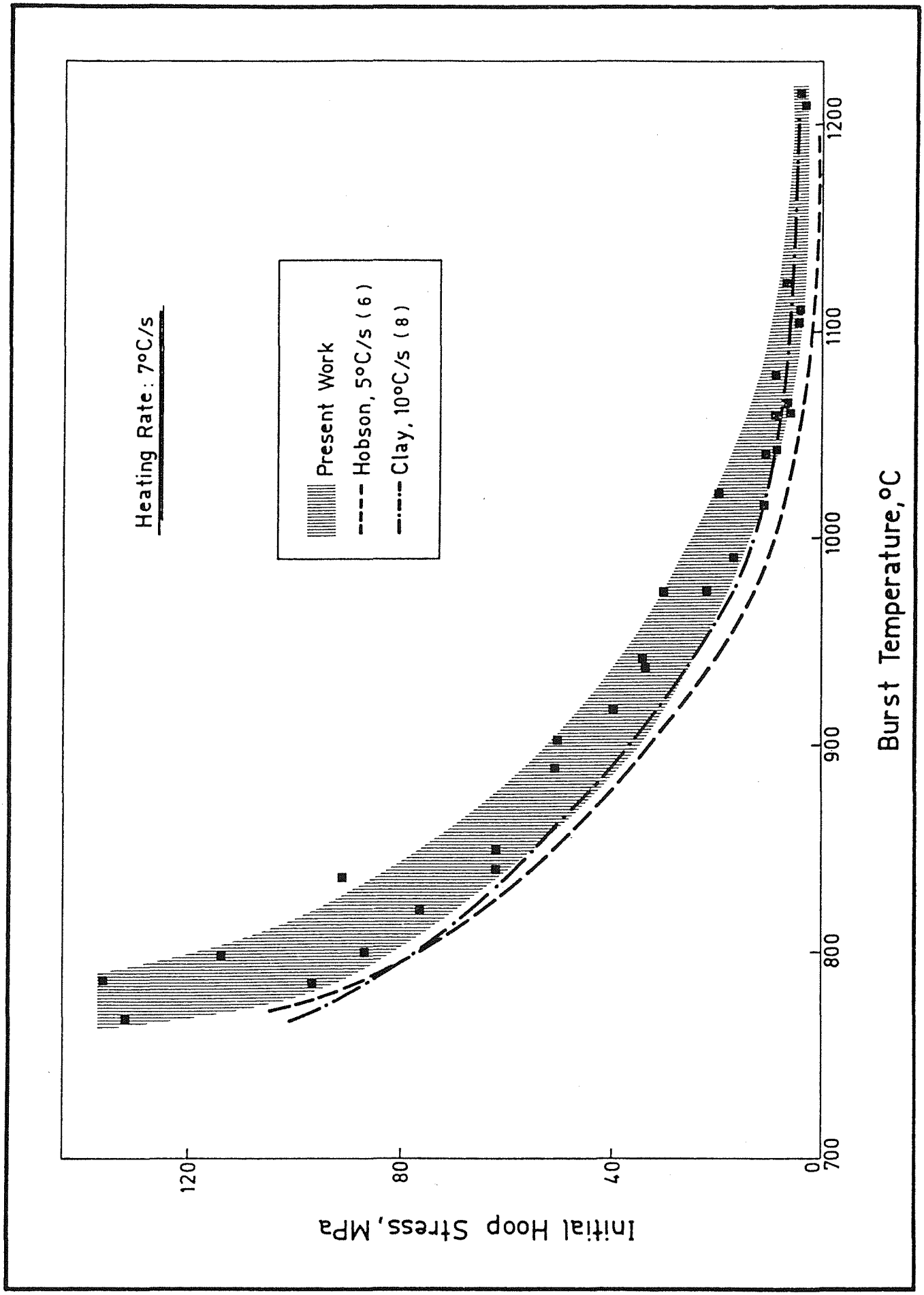

Fig. 25: Comparison of initial hoop stress versus burst temperature with other experimental works. Heating rate 7 K/s

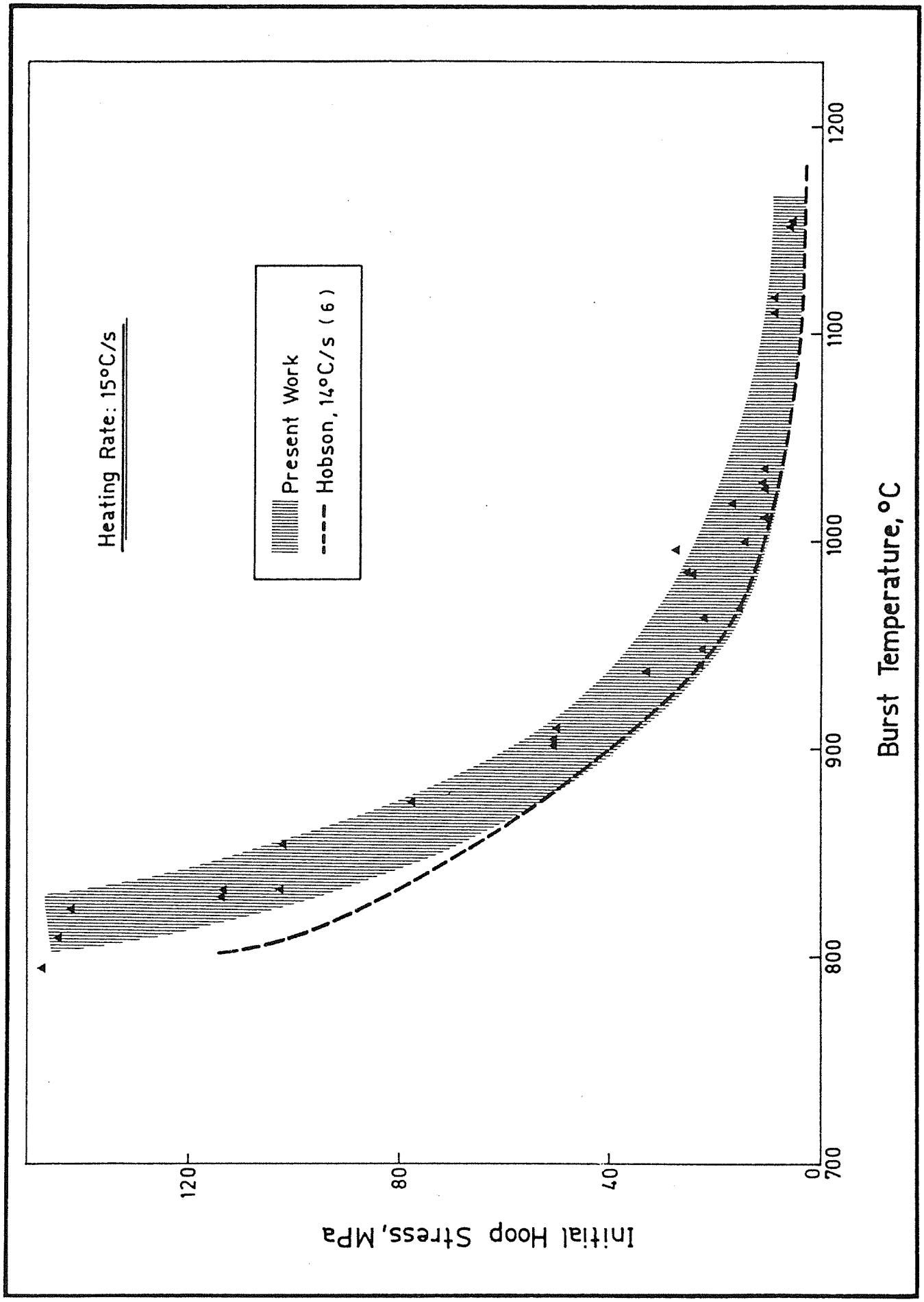

Fig. 26: Comparison of initial hoop stress versus burst temperature with other experimental works. Heating rate 15 K/s